Ghrelin Action in the PVH of Male Mice: Accessibility, Neuronal Targets, and CRH Neurons Activation

Gimena Fernandez, Pablo N de Francesco, María P Cornejo, Agustina Cabral, Julieta P Aguggia, Victor J Duque, Nilufer Sayar, Sonia Cantel, Juan I Burgos, Jean-Alain Fehrentz, et al.

Ghrelin action in the PVH of male mice: accessibility, neuronal targets and CRH neurons activation

Gimena Fernandez[1], Pablo N. De Francesco[1], María P. Cornejo[1], Agustina Cabral[1], Julieta P. Aguggia[1], Victor J. Duque[2], Nilufer Sayar[3], Sonia Cantel[4], Juan I. Burgos[5,#], Jean-Alain Fehrentz[4], Rodrigo Rorato[2], Deniz Atasoy[3], André S. Mecawi[2], Mario Perello[1,6]

[1]Laboratory of Neurophysiology of the Multidisciplinary Institute of Cell Biology [IMBICE, Argentine Research Council (CONICET) and Scientific Research Commission, Province of Buenos Aires (CIC-PBA), National University of La Plata], La Plata, Buenos Aires, Argentina.
[2]Department of Biophysics, Escola Paulista de Medicina, Universidade Federal de São Paulo (UNIFESP), São Paulo, São Paulo, Brazil.
[3]Department of Neuroscience and Pharmacology, Carver College of Medicine, Iowa Neuroscience Institute and Fraternal Order of Eagles Diabetes Research Center (FOEDRC), University of Iowa, Iowa City, Iowa, USA.
[4]Institut des Biomolécules Max Mousseron, Univ Montpellier, CNRS, ENSCM, Montpellier, France.
[5]Centro de Investigaciones Cardiovasculares "Dr. Horacio Eugenio Cingolani" (CONICET and National University of La Plata), La Plata, Buenos Aires, Argentina.
[6]Department of Surgical Sciences, Functional Pharmacology and Neuroscience, University of Uppsala, Uppsala, Sweden.

Corresponding Author:
Dr. Mario Perelló
ORCID ID: 0000-0003-2114-6765
Laboratory of Neurophysiology, Multidisciplinary Institute of Cell Biology
Calle 526 S/N entre 10 y 11-PO Box 403. La Plata, Buenos Aires, Argentina 1900
Phone +54 221 4210112
Email: mperello@imbice.gov.ar

The authors have nothing to disclose.

Short title: Ghrelin actions in the mouse PVH

Keywords: GHSR, hypothalamus, PVN, stress, CRF, HPA axis.

[#]Current address : Multidisciplinary Institute for Investigation in Pediatric Pathologies (IMIPP), Immunology division, CONICET- Government of the City of Buenos Aires (GCBA), Ricardo Gutierrez Children's Hospital, Buenos Aires, Argentina.

ABSTRACT

The hormone ghrelin displays several well-characterized functions, including some with pharmaceutical interest. The receptor for ghrelin, the growth hormone secretagogue receptor (GHSR), is expressed in the hypothalamic paraventricular nucleus (PVH), a critical hub for the integration of metabolic, neuroendocrine, autonomic and behavioral functions. Here, we performed a neuroanatomical and functional characterization of the neuronal types mediating ghrelin actions in the PVH of male mice. We found that fluorescent-ghrelin mainly labels PVH neurons immunoreactive for nitric oxide synthase 1 (NOS1, which catalyze the production of nitric oxide - NO). Centrally-injected ghrelin increases c-Fos in NOS1 PVH neurons and NOS1 phosphorylation in the PVH. We also found that a high dose of systemically-injected ghrelin increases ghrelin level in the cerebrospinal fluid and in the periventricular PVH, and induces c-Fos in NOS1 PVH neurons. Such high dose of systemically-injected ghrelin activates a subset of NOS1 PVH neurons, which does not express oxytocin, via an arcuate nucleus-independent mechanism. Finally, we found that pharmacological inhibition of NO production fully abrogates ghrelin-induced increase of calcium concentration in corticotropin-releasing hormone neurons of the PVH whereas it partially impairs ghrelin-induced increase of plasma glucocorticoid levels. Thus, plasma ghrelin can directly target a subset of NO-producing neurons of the PVH that is involved in ghrelin-induced activation of the hypothalamic-pituitary-adrenal neuroendocrine axis.

INTRODUCTION

Ghrelin is a stomach-derived peptide hormone that acts via the growth-hormone secretagogue receptor (GHSR) [1,2]. Due to its ability to release growth hormone (GH), ghrelin (or ghrelin mimetics) rapidly emerged as promising candidates to enhance GH secretion and consequently treat a variety of conditions, such as preventing the deleterious effects of aging on the GH axis [3]. Moreover, the finding that ghrelin is the most potent known orexigenic hormone has expanded the potential pharmacological implications for ghrelin mimetics as viable therapeutic options in the management of anorexia and cancer-induced cachexia [4]. However, ghrelin treatment also displays a variety of undesirable effects, including increments of glycemia, glucocorticoid levels and fat mass as well as a reduction in insulin sensitivity [3,5]. The neurobiological substrates that mediate some effects of ghrelin are only partially known, and consequently, it is uncertain if such actions can be independently manipulated. For instance, GHSR is expressed in the hypothalamic paraventricular nucleus (PVH), a critical brain center that integrates diverse physiological functions. Surprisingly, however, little is known about the neurobiological basis mediating ghrelin's actions in the PVH.

The PVH contains a variety of molecularly defined neuronal populations that display different metabolic, neuroendocrine, autonomic and behavioral functions [6]. PVH neurons are classified into magnocellular, which mainly project to the posterior pituitary, and parvocellular that project to the median eminence or autonomic control centers [7]. Furthermore, PVH neurons can synthesize different neuropeptides, including vasopressin (AVP), oxytocin (OXT), corticotropin-releasing hormone (CRH), thyrotropin-releasing hormone (TRH) or neurotensin (NT), hereafter named PVH^{AVP}, PVH^{OXT}, PVH^{CRH}, PVH^{TRH} or PVH^{NT} neurons, respectively. PVH neurons also synthesize neurotransmitters such as nitric oxide (NO), norepinephrine or gamma-aminobutyric acid (GABA); these neurons can be recognized by the expression of specific enzymes such as nitric oxide synthase 1 (NOS1), tyrosine hydroxylase (TH) or glutamate decarboxylase 2 (GAD2), hereafter named PVH^{NOS1}, PVH^{TH} or PVH^{GAD2} neurons, respectively. Some PVH neurons show a dual phenotype. For instance, PVH^{OXT} neurons may also be PVH^{NOS1} neurons and, consequently, are referred to as $PVH^{OXT/NOS1}$ neurons [8–11]. The PVH neurons are targeted by ghrelin in mice, which are an instrumental animal model to delineate the neurobiological basis mediating ghrelin's actions in mammals [12]. Studies using *in situ* hybridization [13–15], binding of fluorescently-labeled ghrelin [16] or a reporter mouse [17] have shown that the mouse PVH contains GHSR-expressing neurons (hereafter named PVH^{GHSR} neurons). In mice, systemically-injected ghrelin activates PVH neurons, as indicated by the assessment of the expression of the marker for transcriptional activity

c-Fos, magnetic resonance or positron emission tomography [18–21]. To the best of our knowledge, however, the neurochemical identity of the PVH^{GHSR} neurons is unknown.

The local action of ghrelin in the mouse PVH displays selective effects [12]. For instance, intra-PVH-injected ghrelin does not induce food intake in mice, but activates the hypothalamic-pituitary-adrenal axis (HPA) in a similar extent as seen in response to systemically or centrally-injected ghrelin [22]. Ghrelin does not directly act on PVH^{CRH} neurons, as they do not express GHSR [22], but rather reduces the inhibitory post-synaptic currents in PVH^{CRH} neurons by acting at presynaptic GABA terminals [23,24]. Conversely, ghrelin was shown to inhibit unidentified mouse PVH neurons by decreasing the excitatory inputs in an endocannabinoid-dependent manner [25]. Thus, ghrelin's action in the mouse PVH seems to involve complex local neuronal circuits and molecular mechanisms, whose intricacies have been poorly elucidated.

Ghrelin's actions in the mouse hypothalamus are restricted due to the limited accessibility of this hormone into the brain [26,27]. In particular, plasma ghrelin does not cross the blood-brain barrier [28], and rather only diffuses through fenestrated capillaries of the median eminence in order to reach the neighboring hypothalamic arcuate nucleus (ARH) [24,29]. In the ARH, ghrelin activates the agouti-related peptide (AgRP) neurons (hereafter named ARH^{AgRP} neurons) that, in turn, strongly innervate the PVH [30–33]. Ghrelin can also act in the PVH via ARH-independent mechanisms since systemically-injected ghrelin induces c-Fos expression in the PVH of ARH-ablated mice [24]. It is currently unknown if plasma ghrelin can directly target the PVH. The PVH contains the highest density of capillaries in the hypothalamus [34]; thus, plasma ghrelin may locally diffuse into the PVH in a physiologically significant extent. Since ghrelin crosses the blood-cerebrospinal fluid (CSF)-barrier [35], plasma ghrelin could also target the PVH from the CSF. Here, we first mapped the localization of PVH^{GHSR} neurons in the mouse brain and established its identity. Since we found that a significant fraction of mouse PVH^{GHSR} neurons are $PVH^{OXT/NOS1}$ or PVH^{NOS1} neurons, we investigated if plasma ghrelin can reach and activate them in an ARH-independent manner. Finally, we tested the hypothesis that ghrelin-induced indirect activation of the PVH^{CRH} neurons involves NO signaling.

METHODS

Mice. Studies were performed using wild-type (WT) C57BL/6 mice as well as ARH-intact or ARH-ablated mice, which were generated using subcutaneous (SC) injections of saline alone or containing monosodium glutamate (Sigma-Aldrich, cat# G1626, 2.5 mg/g body weight (BW)), respectively, in 4-day-old WT mice. The ARH was analyzed at the end of the experiments using thionin staining and AgRP immunostaining, and was confirmed to be similarly lesioned in all monosodium glutamate-treated mice, as previously described [20,32,36]. Also, we used Gad2^{tdTomato} mice, which express tdTomato in Gad2-expressing GABA cells, and were generated by crossing Ai14 reporter mice (Allen Institute, 129S6-Gt(ROSA)26Sor$^{tm14(CAG-tdTomato)Hze}$/J; Stock# 007908, [37]) and Gad2-CreER mice (Jackson Laboratory, Gad2$^{tm1(cre/ERT2)Zjh}$/J; Stock# 010702, [38]) that express a tamoxifen-inducible Cre recombinase under the endogenous promoter of Gad2 gene. Adult Gad2^{tdTomato} mice received daily injections of tamoxifen (Sigma-Aldrich, cat# T5648; 70 mg/kg BW, intraperitoneal, IP) for 4 consecutive days to induce Cre recombination, and used 3 weeks later. Also, we used 4 Crh-IRES-Cre mice, which express Cre recombinase under the promoter of *Crh* gene (Jackson Laboratories, B6(Cg)-Crh$^{tm1(cre)Zjh}$/J, Stock# 012704, [38]). All mice were backcrossed for more than 10 generations onto a C57BL/6 genetic background. Experimental mice were 10-14-week-old males that were maintained under controlled temperature (22±1°C) and photoperiod (12-h light cycle from 7:00 am to 7:00 pm). Five days before the experimental day, mice were individually housed and *ad libitum* fed with regular chow diet, which was available until the time of anesthesia/treatment and then taken away. The protocols received approval from the Institutional Animal Care and Use Committee of the IMBICE, UNIFESP and the FOEDRC, where the mouse studies were performed.

Labeling with fluorescent ghrelin. PVH cells directly responsive to ghrelin were labeled with far red-ghrelin (Fr-ghrelin), which is a variant of ghrelin conjugated to DY-647P fluorophore at its C-terminal end [39]. We have shown that centrally-administered fluorescent ghrelin in mice selectively labels GHSR-expressing neurons present in periventricular hypothalamic nuclei, including not only the PVH but also the ARH, the ventromedial nucleus and the dorsomedial nucleus [16, 39]. Anesthetized mice were stereotaxically implanted with a single indwelling guide cannula (4-mm long, 22-gauge, PlasticsOne) into the lateral ventricle (coordinates: 0.34 mm anterior; ±1 mm lateral and 2.3 mm ventral) and intracerebroventricularly (ICV) injected with 2 µL of Fr-ghrelin (60 pmol/mouse, which is minimum amount of tracer that can be directly visualized). Central injections were made over 2 min through a 30-gauge needle. Mice were perfused with formalin after 30 min. Brains were removed, post-fixed, immersed in 20% sucrose, and coronally

cut into four equal 40-µm series on a cryostat. Correct location of cannulas was confirmed by histological observation at the end of experiments. Here, we used (a) naïve WT mice (n=12), (b) WT mice that were ICV-injected with colchicine (16 µg/mouse) 2-day before the experiment (n=3), and (c) Gad2^{tdTomato} mice (n=3).

Immunolabeling of the subsets of PVH neurons. In order to reveal the identity of PVH cells labeled by Fr-ghrelin, one series of brain sections containing the PVH of mice ICV-injected with Fr-ghrelin were treated with blocking solution (2% normal donkey serum and 0.25% Triton X-100 in PBS). Brain sections of WT mice were incubated with the following antibodies: rabbit anti-TH (Santa Cruz Biotechnology, Cat# sc-14007, 1:5000, RRID: AB_671397), rabbit anti-NOS1 (Thermo Fisher Scientific, Cat# 61-7000, 1:3000, RRID: AB_2313734), mouse anti-neurophysin I (marker of PVH^{OXT} neurons, National Institute of Neurological Disorders and Stroke (NINDS), Cat# PS38, 1:1000, RRID: AB_2315026), or mouse anti-neurophysin II (marker of PVH^{AVP} neurons, NINDS, Cat# PS41, 1:1000, RRID: AB_2313960). Brain sections of colchicine-treated mice were incubated with the following antibodies: goat anti-CRH (recognizes CRH [40], Santa Cruz Biotechnology, Cat# sc-1759, 1:500, RRID: AB_631300), rabbit anti-TRH (recognizes proTRH [41], 1:500, RRID: AB_2315485) or rabbit anti-NT (ImmunoStar, Cat# 20072, 1:1000, RRID: AB_572254). In order to label PVH$^{OXT/NOS1}$ neurons, subsets of sections were simultaneously incubated with antibodies against neurophysin I and NOS1. After 48 h at 4°C, sections were incubated with donkey anti-rabbit AlexaFluor594 (Thermo Fisher Scientific, Cat# A-21207, 1:1000, RRID: AB_141637), donkey anti-mouse AlexaFluor594 (Thermo Fisher Scientific, Cat# A-21203, 1:1000, RRID: AB_141633) or donkey anti-goat AlexaFluor594 (Thermo Fisher Scientific, Cat# A-11058, 1:1000, RRID: AB_2534105) secondary antibodies, depending on the primary antibody used in each case, for 2 h at room temperature. Finally, slices were mounted on glass slides and coverslipped with mounting media.

scRNA-seq data analysis. Raw and processed scRNA-Seq datasets of fluorescent GFP+ PVH neurons isolated from mice generated by crossing an Oxt-Flp recombinase driver line to a Flp-dependent GFP reporter line [42] were analyzed to identify Ghsr expressing neurons. Quality control (QC) assessment and cell clustering were preserved from the original analysis. Starting with 146 QC-accepted neurons, cells were classified as *Ghsr*+, *Oxt*+ and/or *Nos1*+ based on their respective transcript counts being greater than zero. Subsequently, they were grouped and counted according to the resulting joint positivity, along with their original magnocellular or parvocellular classification. Analysis was performed in RStudio 2023.06.0, R version 4.3.0. Original datasets are publicly available at https://github.com/gofflab/OT_neuron_study_2020.

Central injection of ghrelin. WT mice were implanted with a single indwelling ICV guide cannula into the lateral ventricle using stereotaxic surgeries, as described above. Here, the guide cannulas were permanently attached to the skull with dental cement and plugged with a 28-gauge dummy cannula. After surgery, mice were allowed to recover for at least 5 days. During these days, mice were accustomed to handling and removal of the dummy cannula. At around 9:30−10:00 am of the experimental day, mice were ICV-injected with 2 µL of artificial CSF alone or containing ghrelin (Global Peptide, cat# PI-G-03, 60 pmol/mouse). Mice were anesthetized and perfused at 120 min after treatment for c-Fos immunostaining (n=4 and 4 for vehicle or ghrelin, respectively) or at 15, 30 and 120 min after treatment for phospho-NOS1 immunostaining (n=3 for vehicle, and n=4, 3 and 3 for ghrelin, respectively). Brains of perfused mice were obtained and used to generate coronal sections for immunostainings, as described above. An independent set of cannulated WT mice were ICV-injected with 2 µL of artificial CSF alone (n=6) or containing 60 pmol/mouse of ghrelin (n=6) and euthanized 30-min post-treatment. Here, brains were obtained and cut in coronal sections in order to obtain PVH punches, which were, in turn, used to isolate total RNA (see below). In all cases, the correct location of ICV injections was verified at the end of the experiment by histological analysis.

Systemic injection of ghrelin. For dose-response studies, WT mice were SC-injected with saline alone or containing ghrelin (60 or 600 pmol/g BW). Mice were perfused, as described above, at 120-min post-treatment for c-Fos immunostaining (n= 5, 8 and 3 per group, respectively) or anesthetized at 10-min post-treatment for CSF extraction. In the latter case, anesthetized mice were placed in a stereotaxic frame and used to collect CSF from the cisterna magna at 30-min post-treatment, as recently reported [39]. CSF samples were collected on EDTA (1 mg/mL final) and p-hydroxy-mercuribenzoic acid (0.4 mM final) and acidified with HCl (0.1 M final). Ghrelin was assessed in pools of 30 µL of CSF (n=4 per group). An independent set of WT mice were SC-injected with vehicle alone (n=4) or containing 600 pmol/g BW of fluorescein-ghrelin (F-ghrelin, n=4). F-ghrelin is a 19-residue analog of ghrelin conjugated to fluorescein isothiocyanate at its C-terminal end [16,43]. These mice were anesthetized and perfused at 20-min post-treatment, and their brains were processed for immunostainings against fluorescein (see below).

Two additional experiments were performed to further study the action of the high dose of ghrelin in the PVH. A set of ARH-intact and ARH-ablated mice were SC-injected with vehicle (n=4 per group) or ghrelin (600 pmol/g BW, n=4 per group), anesthetized and perfused 120-min post-treatment. These brains were processed for c-Fos, NOS1 and neurophysin I immunostainings (see below). Another cohort of WT mice was SC-treated with vehicle alone or containing either ghrelin

(600 pmol/g BW), N-nitro-L-Arginine methyl ester (L-NAME, 10 µg/g BW), or a combination of both. Mice were euthanized at 120-min post-treatment for c-Fos immunostainings (n=3, 4, 3 and 8 per group, respectively) or at 30-min post-treatment to obtain both PVH punches for mRNA quantification and blood samples for corticosterone assessment (n= 9, 8, 9 and 7 per group, respectively).

Chromogenic immunostaining. For c-Fos, phospho-NOS1 or fluorescein immunostaining, one series of sections were pretreated with 0.5% H_2O_2, next treated with blocking solution and then incubated with the following antibodies: rabbit anti-c-Fos antibody (Millipore, Cat# PC38, 1:20.000, RRID: AB_2106755), rabbit anti-phospho-NOS1 (Abcam, Cat# ab5583, 1:1500, RRID: AB_304964) or goat anti-fluorescein (Molecular Probes, Cat# A-11096, 1:1500, RRID: AB_221558) for 48 h at 4°C. Then, sections were incubated with biotinylated donkey anti-rabbit (Jackson ImmunoResearch Labs, Cat# 711-065-152, 1:3000, RRID: AB_2340593) or biotinylated rabbit anti-goat (Vector Laboratories, Cat# BA-5000, 1:1500, RRID: AB_2336126) secondary antibodies depending on the primary antibody used in each case, for 1 h at room temperature and then treated with avidin-peroxidase complex (Vectastain Elite ABC kit, Vector Laboratories, Cat# PK-6200) for 1 h, according to manufacturer's protocols. Finally, sections were incubated with 3-3′-diaminobenzidine (Sigma-Aldrich, Cat# D8001)/Nickel solution in order to generate a black/purple precipitate in immunoreactive cells. Afterward, sections were sequentially mounted on glass slides and coverslipped with mounting media. For triple immunostaining against c-Fos, neurophysin I and NOS1, brain sections were first subjected to chromogenic immunostaining against c-Fos and then to fluorescent immunostaining against neurophysin I and NOS1, as described above.

Imaging and quantitative analysis. Images were acquired with 20x/0.80 and 40x/0.95 objectives using a Zeiss AxioObserver D1 equipped with an Apotome.2 structured illumination module and an AxioCam 506 monochrome camera. For samples subjected to chromogenic immunostaining alone, bright-field images were acquired using a Nikon Eclipse 50i and a DS-Ri1 Nikon digital camera with a 0.45X adapter using 10X/0.3 and 60X/0.80 objectives. Images were taken in comparable areas and under the same optical and light conditions. Image processing and analysis were performed in the ImageJ-based open-source image-processing package Fiji [44]. Quantitative analyses were performed in sections containing the PVH (between bregma -0.58 and -1.22 mm) or ARH (between bregma -1.58 and -2.06 mm) that were identified using the mouse brain atlas [45]. Quantifications were bilaterally performed and corrected by double counting. The total number of labeled cells in each area was determined by multiplying the number of cells

counted by four to correct for uncounted sections of the nucleus. Additionally, data were corrected using the Abercrombie method [46], which takes into account the thickness of the sections and the mean diameter of the neuron along the z-axis. The mean diameter of the neurons was determined using Fiji.

The number of cells labeled with Fr-ghrelin (hereafter Fr-ghrelin+ cells) within the PVH was expressed as total Fr-ghrelin+ cells per PVH. For the phenotypical characterization of Fr-ghrelin+ PVH cells, the fraction of Fr-ghrelin+ cells positive for each marker or set of markers were expressed as a percentage, which represents the fraction of Fr-ghrelin+ cells and a given marker (or markers) as compared to the total number of either Fr-ghrelin+ cells or cells positive for a given marker (or markers). The number of phospho-NOS1+ cells was expressed per PVH section per side. The total number of c-Fos+ in the ARH or the PVH was expressed per PVH section per side, whereas the fraction of c-Fos+ cells of a given cell type are shown as a percentage versus the total number of the given cell type in the PVH, or in a subregion of the PVH (e.g., periventricular vs. lateral regions of the PVH). The diffusion of F-ghrelin within the PVH was measured as described in detail in the past [35]. Briefly, bright-field images were converted into 16-bit images. Images underwent flat-field correction, and the pixel intensity values were transformed into optical density data by taking the negative decimal logarithm of the original value divided by the flat-field value. Optical density profiles were acquired perpendicular to the 3V along the length of a 300-µm box at the PVH level. The average optical density of a 25-µm region farthest from the 3V was subtracted from each profile, and the resulting curve was aligned using the first zero-crossing point nearest to the 3V. The software Fiji was employed for all image processing and analysis steps.

qPCR for RNA quantification in PVH punches. After euthanasia, brains were rapidly removed, frozen on dry ice and stored at –80°C. Brains were sliced into 60-µm coronal sections using a cryostat. The PVH was identified, according to the mouse brain atlas [45], and collected using a 500-µm micropunch needle. The punch location was confirmed by toluidine blue (0.1%) staining of the sections. PVH punches were collected in TRIzol® reagent, and total RNA was extracted following the manufacturer's instructions. RNA concentration was measured using a NanoDrop™ One spectrophotometer. Samples were diluted to the same concentration and treated with the DNase I Amp Grade kit (Life Technologies) to eliminate genomic DNA. RNA integrity was confirmed by the detection of 18S and 28S bands after agarose-formaldehyde gel electrophoresis (not shown), and RNA quality was verified by optical density absorption ratio 260 nm/280 nm. The cDNA was synthesized using the QuantiTect Reverse Transcription Kit (Qiagen) using 300 ng of total RNA. The optimization and validation of primers were performed using a qPCR standard curve. Primers used were: sense: 5′-AGCATGGGCTCTCCTGTCA-3′, antisense: 5′-

GAGACCAGAGTGGGCTGCA-3′ for *c-Fos*; sense:5′-TCAAAGCCATCCAGCGCATA-3′, antisense: 5′-GGTACCGGTTGTCATCCCTC-3′ for *Nos1*; sense: 5′-TGCCCCAGTCTTGCTTGCT-3′, antisense: 5′-TCCAGGTCTAGCGCAGCCC-3′ for *Oxt*; and sense: 5′-GAAGGTCAAAGGGAATGTGTTCA-3′, antisense: 5′-CCTTGTCTGCCTTCAGCTTGT-3′ for *Rpl19*. Samples were 1:5 diluted and qPCRs were performed in triplicate using SYBR green (Applied Biosystems) in a QuantStudio™ 5 Real-Time PCR System, with 384-well following the manufacturer's instructions. The ribosomal protein L19 mRNA (*Rpl19*) did not show statistical differences among groups and was used as an internal control gene for the assays. For relative quantification of gene expression, the 2−ΔΔCT method was employed.

ELISA: CSF ghrelin concentration was assayed using a specific ghrelin ELISA kit (Bertin Pharma, cat# A05117, RRID: AB_2619624, intra-assay variation 8.1%), whose detection limit was 6.7 pg/mL. For corticosterone assessment, blood samples were collected in EDTA-coated tubes, and plasma was obtained after centrifugation and stored at −20°C. Plasma corticosterone concentration was determined using a competitive ELISA (Arbor Assays, cat# K014-H1, RRID: AB_2877626, intra-assay variation 5.2%).

In vivo calcium imaging. Here, anesthetized Crh-IRES-cre mice were stereotaxically-injected with 300 to 500 nL of AAV-CAG-FLEX-GCaMP8m (Addgene, #162381) virus in both PVH (coordinates: 0.8 mm anterior, ±0.2 mm bilateral, 5.6 mm ventral) using a pulled glass pipette controlled by a micromanipulator. Next, a metal ferrule-capped optical fiber (400 µm core diameter, NA=0.48, Thorlabs) was implanted ~100 µm above the viral injection site in the midline and ferrules were fixed with dental cement. After 5-6-week recovery, Crh-IRES-cre mice were single-housed in custom plexiglass cages. After 1-2 days of habituation, mice were tethered to the optical fiber (400 µm core, 0.48 NA, bundled fibers, Doric Lenses) and allowed to acclimatize for a few hours before the starting experiments. Signals from 405 nm and 465 nm excitation (at 30-50 µW) were acquired at a 3 Hz sampling rate with Doric FP Bundle Imager (Doric Lenses). Recordings were performed in the absence of food in otherwise *ad libitum* fed animals. After 30 min baseline recording, mice were systemically injected with vehicle, different doses of ghrelin (60 or 600 pmol/g BW) and a high dose of ghrelin (600 pmol/g BW) plus L-NAME (10 µg/g BW) under brief (5 sec) anesthesia with isoflurane. For the analysis of the fiber photometry data, the isosbestic signal (405 nm) was fit to the calcium-dependent (465 nm) signal using the linear least squares fit in a custom MATLAB script. ΔF/F was calculated as (465 nm–fitted 405 nm)/(fitted 405 nm), and from these values, z-scores were calculated for the baseline period to account for the inter-animal differences in signal intensities (F-µ)/δ where F is the calculated ΔF/F value, µ and δ are the mean and standard

deviation for the baseline period, respectively. After the *post hoc* analysis, mice were eliminated from the analyses if the fiber tip location and/or sensor expression were off-target.

Statistical analyses. Normality and homogeneity of variances were tested using the D'Agostino & Pearson omnibus test or Bartlett's test, respectively. Data were expressed as the mean ± standard error of the mean (SEM), and the experimental groups were compared with Student's unpaired t-test, One-sample t-test or One-way ANOVA, depending on the number of groups or experimental design. Tests used for each comparison and statistical outputs are indicated in the figure legends or the text depending if data summaries are shown as text or graphs, respectively. Differences were considered significant when $p<0.05$. All statistical analyses were conducted with the software GraphPad Prism, version 9.0.

RESULTS

1) Ghrelin directly targets OXT/NOS1+ cells of the PVH. We first performed a systematic analysis of the number and the localization of PVH cells that were labeled in mice ICV-injected with Fr-ghrelin. Fr-ghrelin labels 789±20 cell bodies in the mouse PVH that were located between bregma -0.58 and -1.22 mm of the Paxinos brain atlas **(Figure 1A-B)**. Fr-ghrelin+ cells were present in all sub-regions of the PVH, and the majority of them (718±19) were enriched in the anteromedial part of the nucleus, between bregma -0.58 and -0.94 mm **(Figure 1B)**. Fr-ghrelin+ cells were relatively homogeneous in shape, with 15.8±0.3 µm of diameter **(Figure 1C)**. Strikingly, Fr-ghrelin+ signal was also observed in fiber-like structures that were enriched in the periventricular region of the PVH, and laterally-oriented **(Figure 1D-E)**. In terms of the neurochemical phenotype of the Fr-ghrelin+ cells **(Figure 1F)**, Fr-ghrelin did not label PVH^{CRH}, PVH^{TRH} or PVH^{NT} neurons in brain sections of colchicine-treated mice. In $Gad2^{tdTomato}$ mice, PVH^{GAD2} cells represented 1.0±0.6% of all Fr-ghrelin+ cells. In naïve mice, PVH^{NOS1}, PVH^{OXT}, PVH^{AVP} and PVH^{TH} neurons represented 42.2±4.5, 37.1±4.0, 7.0±2.7 and 1.4±0.8 % of all Fr-ghrelin+ cells.

Since $PVH^{OXT/NOS1}$ neurons exist in the mouse hypothalamus [8–11], we assessed if they were labeled by Fr-ghrelin **(Figure 2A)**. We found that $PVH^{OXT/NOS1}$ neurons were enriched in the anteromedial part of the nucleus and represented 74.2±4.8% of all PVH^{NOS1} neurons and 83.4±7.3% of all PVH^{OXT} neurons, in agreement with previous reports [8–11]. Fr-ghrelin labeled 258±17, 107±17 and 70±7 $PVH^{OXT/NOS1}$, PVH^{NOS1} and PVH^{OXT} neurons, respectively. Thus, Fr-ghrelin labeled 22.2±7.0, 11.9±6.1 and 29.3±10.4 % of all $PVH^{OXT/NOS1}$, PVH^{NOS1} and PVH^{OXT} neurons, respectively, which represented 32.6±6.1, 9.8±5.2 and 7.6±2.8 % of all Fr-ghrelin+ cells (~50% all Fr-ghrelin+ cells, **Figure 2B**). In order to clarify the nature of the $PVH^{OXT/NOS1}$ and PVH^{OXT} neurons targeted by ghrelin, we analyzed a dataset of the transcriptional profile of OXT-producing neurons that was obtained by scRNA-seq analysis of the cells expressing green fluorescent protein (hereafter named GFP+ cells) collected from PVH samples of OXT-reporter mice systemically injected with fluorogold to label magnocellular neurons [42]. The analysis of the transcriptional profile of 146 GFP+ cells reported in the mentioned study revealed that *Ghsr* was expressed in 9 GFP+ cells, all of which were magnocellular PVH cells **(Figure 2C-D)**, as indicated by the transcriptional profile and the presence of fluorogold. Six of the 9 GFP+ cells expressing *Ghsr* also express *Nos1* **(Figure 2E).** Thus, *Ghsr* was expressed in ~7.1 and ~9.4 % of all $PVH^{OXT/NOS1}$ and PVH^{OXT} neurons, respectively **(Figure 2F)**.

2) Centrally-injected ghrelin acts on PVH$^{OXT/NOS1}$, PVH^{NOS1} and PVH^{OXT} neurons. Since centrally injected ghrelin induces c-Fos in the PVH [22], we tested if centrally-injected ghrelin activates PVH$^{OXT/NOS1}$, PVH^{NOS1} and PVH^{OXT} neurons. We found that ICV-injected ghrelin increased the fraction of PVH$^{OXT/NOS1}$ (35.5±1.4 vs. 0.2±0.1 % of all PVH$^{OXT/NOS1}$), PVH^{NOS1} (24.4±7.0 vs. 0.0±0.0 % of all PVH^{NOS1}) and PVH^{OXT} (13.6±4.9 vs. 0.0±0.0 % of all PVH^{OXT}) neurons positive for c-Fos, as compared to vehicle treatment ($p<0.05$ for all cases, Student's t-test, **Figure 3A**). Since the phosphorylation of NOS1 at Ser1417 increases its activity and, consequently, the production of NO [47,48], we performed immunostaining against phospho-NOS1 in brain sections of mice ICV-injected with ghrelin **(Figure 3B)**. We found that ICV-injected ghrelin transiently increased the number of phospho-NOS1 positive cells in the PVH, reaching the peak 15 min after treatment **(Figure 3C)**. Conversely, ICV-injected ghrelin increased the mRNA levels of c-*Fos* in the PVH at 30-min post-treatment (1.00±0.16- vs. 1.99±0.22-fold, $p<0.05$, Student's t-test) but it did not affect mRNA levels of *Nos1* and *Oxt* (1.00±0.18- vs. 1.05±0.21-fold and 1.00±0.15- vs. 0.86±0.22-fold, respectively), as compared to vehicle treatment.

3) A high dose of systemically-injected ghrelin is required to activate the PVH. In order to test the extent to which plasma ghrelin can act in the PVH, we systemically-injected WT mice with 60 and 600 pmol/g BW of ghrelin, which induce a ~2.3- and ~16.8-fold transient increase of plasma ghrelin levels at 30-min post-treatment, respectively [20]. At 2-h post-treatment, we confirmed that both doses of ghrelin increase the number of c-Fos+ cells in the ARH (9±2, 44±10 and 129±11 for vehicle, 60 pmol/g of ghrelin and 600 pmol/g of ghrelin, respectively. One way ANOVA, [$F_{treat}(2,13) = 26.11$, $p<0.0001$]), as previously shown [20]. Conversely, only the high dose of ghrelin increased the number of c-Fos+ cells in the PVH (7±2, 8±1 and 153±23 cells/side for vehicle, 60 pmol/g of ghrelin and 600 pmol/g of ghrelin, respectively. One way ANOVA, [$F_{treat}(2,13) = 102.2$, $p<0.0001$], **Figure 4A**). Next, we tested if systemically-injected ghrelin reaches the CSF in our experimental conditions. At 30-min post-treatment, ghrelin was undetectable in the CSF of vehicle-injected mice, as we reported in the past [35], as well as in the CSF of mice injected with 60 pmol/g BW of ghrelin, whereas we detected 29.9±12.3 pg/mL of ghrelin in the CSF of mice injected with 600 pmol/g BW of ghrelin. To assess if the elevation of ghrelin in the CSF could impact the PVH, we systemically-injected 600 pmol/g BW of F-ghrelin in mice and estimated the presence of tracer in this hypothalamic area using immunostaining **(Figure 4B)**. As previously reported, fluorescein signal was mainly detected at the ARH of F-ghrelin injected mice (not shown, [20]). In the PVH, quantitative analysis of optical intensity in the medial-lateral axis at the level of the PVH showed that the F-ghrelin signal was higher at all distances from 0 to ~70 µm from the ventricle wall as well as at some, but not all, distances comprised between the ~70 and 130 µm range, as compared to

vehicle-treated mice **(Figure 4C)**. F-ghrelin signal beyond ~130 µm away from the ventricle wall showed no significant difference between mice injected with vehicle or F-ghrelin. Thus, a high dose of systemically-injected ghrelin is required to investigate the direct effects of the hormone on the PVH.

4) Systemically-injected ghrelin acts on $PVH^{OXT/NOS1}$ and PVH^{NOS1} neurons. Next, we tested if the high dose of systemically-injected ghrelin activates $PVH^{OXT/NOS1}$, PVH^{NOS1} and PVH^{OXT} neurons. We found that ghrelin induced a significant increase in the fraction of $PVH^{OXT/NOS1}$ (26.7±5.2 vs. 1.0±0.6% of all $PVH^{OXT/NOS1}$) and PVH^{NOS1} (25.1±8.3 vs. 0.0±0.0% of all PVH^{NOS1}) neurons positive for c-Fos, as compared to vehicle treatment ($p<0.05$ for all cases, Student's t-test) but did not affect the fraction in PVH^{OXT} neurons positive for c-Fos (6.2±2.1 vs. 0.2±0.2% of all PVH^{OXT}). The high dose of ghrelin increased the mRNA levels of c-*Fos* in the PVH at 30-min post-treatment (1.00±0.26 vs. 2.71±0.86, $p<0.05$, Student's t-test), but it did not affect mRNA levels of *Nos1* and *Oxt* (1.00±0.19- vs. 1.11±0.17-fold and 1.00±0.10- vs. 0.93±0.09-fold, respectively) as compared to vehicle treatment.

In order to test if the ARH is required for the ghrelin-induced increase of c-Fos in $PVH^{OXT/NOS1}$ and PVH^{NOS1} neurons, we assessed c-Fos induction in the hypothalamus of ARH-intact and ARH-ablated mice systemically-injected with 600 pmol/g BW of ghrelin **(Figure 5A)**. Here, we separately estimated the fraction of PVH^{OXT}, $PVH^{OXT/NOS1}$ and PVH^{NOS1} neurons positive for c-Fos in the periventricular and lateral regions of the PVH, since these regions were differentially reached by systemically-injected F-ghrelin. Here, quantitative analysis indicated that all quantified $PVH^{OXT/NOS1}$, PVH^{NOS1} and PVH^{OXT} neurons of vehicle-treated ARH-intact and ARH-ablated mice lacked c-Fos. We found that ghrelin treatment increased the fraction of c-Fos+ $PVH^{OXT/NOS1}$ neurons in both regions of PVH of ARH-intact mice, as compared to basal levels, but not in ARH-ablated mice, in which the fractions of c-Fos+ $PVH^{OXT/NOS1}$ neurons were not different than zero **(Figure 5B-C)**. Conversely, the high dose of ghrelin induced a similar increase in the fraction of c-Fos+ PVH^{NOS1} neurons in each region of PVH of ARH-intact and ARH-ablated mice **(Figure 5D-E)**. Ghrelin did not affect the fraction of PVH^{OXT} neurons positive for c-Fos in any region of the PVH of ARH-intact and ARH-ablated mice **(Figure 5F-G)**. Thus, a high dose of systemically-injected ghrelin activates PVH^{NOS1} via ARH-independent mechanisms and the $PVH^{OXT/NOS1}$ neurons via ARH-dependent mechanisms.

5) Ghrelin-induced activation of hypophysiotropic PVH^{CRH} neurons involves NO signaling. Centrally and systemically-injected ghrelin activates PVH^{CRH} neurons in mice, in an ARH-

447 independent manner [22,24]. Since NO activates PVH^{CRH} neurons [49,50], we hypothesized that ghrelin-
448 induced activation of PVH^{NOS1} and PVH$^{OXT/NOS1}$ neurons could contribute to mediate the stimulatory
449 action of systemically-injected ghrelin on the PVH^{CRH} neurons. Thus, we tested if ghrelin affects
450 calcium levels in PVH^{CRH} neurons using fiber photometry-based calcium assessment in a reporter
451 mouse model that expresses GCaMP8m selectively in such neuron type. We found that 60 pmol/g
452 BW of ghrelin does not affect the calcium signal in PVH^{CRH} neurons, whereas 600 pmol/g BW of
453 ghrelin increased it at the 10- to 20 min post-treatment time period **(Figure 6A-C)**. Notably,
454 simultaneous injection of ghrelin and the NOS inhibitor L-NAME fully abrogated the ghrelin-induced
455 increase of calcium signal in PVH^{CRH} neurons. Additionally, systemically-injected ghrelin did not
456 affect *Crh* mRNA levels in the PVH at 30 min post-treatment (not shown), and we found no
457 evidence that L-NAME affects such ghrelin-induced increase of c-Fos in the PVH **(Figure 6D)**.
458 However, the high dose of ghrelin increased plasma corticosterone concentration in mice treated
459 or not with L-NAME, as compared with their control groups; but the increment was smaller in mice
460 treated with ghrelin and L-NAME **(Figure 6E)** suggesting that L-NAME-mediated impairment of the
461 ghrelin-induced activation of PVH^{CRH} neurons affects the overall activation of the HPA axis.

DISCUSSION

Here, we provide a neuroanatomical and functional characterization of PVH^{GHSR} neurons in male mice. First, we describe that mouse PVH^{GHSR} neurons include $PVH^{OXT/NOS1}$ and PVH^{NOS1} neurons. Then, we show that centrally-injected ghrelin activates $PVH^{OXT/NOS1}$ and PVH^{NOS1} neurons. Conversely, a high, but not a low, dose of systemically-injected ghrelin is required to reach the CSF and further act into the PVH. Such high dose of systemically-injected ghrelin activates $PVH^{OXT/NOS1}$ and PVH^{NOS1} neurons, and ghrelin-induced activation of PVH^{NOS1} neurons occurs in an ARH-independent manner. Thus, only PVH^{NOS1} neurons may be able to directly respond to plasma ghrelin. Finally, we found that pharmacological inhibition of NO production impairs ghrelin-induced activation of PVH^{CRH} neurons suggesting that PVH^{NOS1} neurons play a role mediating the central stimulatory effects of ghrelin on the HPA axis.

We found that PVH^{GHSR} neurons are mainly $PVH^{OXT/NOS1}$ neurons (~33%) or PVH^{NOS1} neurons (~10%) whereas smaller subsets of them are PVH^{OXT} neurons (~8%), PVH^{AVP} neurons (~7%), PVH^{GAD2} neurons (~1%) or PVH^{TH} neurons (~1%). Thus, we revealed the phenotype of ~60% of PVH^{GHSR} neurons. The phenotype of the remaining PVH^{GHSR} neurons remains unknown but may include glutamatergic neurons, which are enriched in the PVH [51–54]. We estimated that the mouse PVH contains ~2000 PVH^{NOS1} neurons and ~1500 PVH^{OXT} neurons, slightly above what was reported in previous reports [6,11,55]. Among these neurons, we found that $PVH^{OXT/NOS1}$ neurons represent ~84% of all PVH^{OXT} neurons and ~63% of all PVH^{NOS1}, estimations that agree with previous reports in mice [11] and in rats, in which the majority of the magnocellular PVH^{OXT} are $PVH^{OXT/NOS1}$ neurons that, in turn, constitute the main PVH^{NOS1} cell type [8,56–58]. Here, we found Fr-ghrelin labels ~370 NOS1+ neurons (including $PVH^{OXT/NOS1}$ and PVH^{NOS1} neurons) and presumably activates them since centrally-injected ghrelin induces c-Fos expression in both neuron types as well as NOS1 phosphorylation that enhances its enzymatic activity [47,48]. Thus, it seems reasonable to hypothesize that ghrelin induces local PVH NO production, although this parameter was not assessed. We could not identify if Fr-ghrelin labels magnocellular or parvocellular PVH neurons, as these cell types are intermingled in the mouse PVH and are hard to discriminate without additional assessments [6]. However, the analysis of a scRNAseq dataset revealed that *Ghsr* expression is enriched in magnocellular PVH^{OXT} neurons that, in turn, are mainly $PVH^{OXT/NOS1}$ neurons [42]. Thus, current neuroanatomical and transcriptomic analyses indicate that ghrelin can directly target subsets of $PVH^{OXT/NOS1}$ and PVH^{NOS1} neurons. Of note, neuroanatomical analyses indicated that ghrelin targets larger fractions of each neuronal subset as compared to the estimations based on the transcriptomic analyses. Neuroanatomical analyses are presumably

more reliable as they are based on a larger sample size (~1800 cells/mouse in 5 mice vs. 146 total cells). Transcriptomic analyses, in turn, have likely underestimated the number of Ghsr-expressing cells due to low gene expression/copy number of *Ghsr* compared to a typical single-cell sequencing depth. Indeed, low recovery rates of Ghsr-expressing cells in other available scRNAseq datasets that included hypothalamic cells [53,59] prevented us from performing additional analysis of the subsets of PVH neurons directly responsive to ghrelin.

Our results indicate that high plasma ghrelin concentrations, as those detected under calorie restricted mice [20,36], are required to activate NO-producing neurons of the PVH. In particular, we found that only high (~16.8-fold at 30-min post-treatment), but not low transient elevations in plasma ghrelin concentration increase c-Fos expression in the entire PVH and specifically in $PVH^{OXT/NOS1}$ neurons and PVH^{NOS1} neurons. The observations that only the administration of the higher dose of systemically-injected ghrelin (or F-ghrelin) induces detectable levels of ghrelin in the CSF, and leads to the presence of the tracer in the periventricular region of the PVH, with a medial-to-lateral diffusion pattern, suggest that ghrelin needs to cross the blood-CSF-barrier and reach the CSF in order to act in the PVH, as we have shown for other brain targets [27]. Notably, we also found here that centrally-injected fluorescent ghrelin labels fibers in the periventricular region of the PVH. Although the identity of these fibers was not revealed, a previous study showed that magnocellular $PVH^{OXT/NOS1}$ neurons of rats send processes that break through the ependymal layer of the third ventricle and contact the CSF [60]. Thus, ghrelin-induced activation of the PVH may also involve some direct sensing of ghrelin present in the CSF. At the functional level, we found that systemically-injected ghrelin increases c-Fos in PVH^{NOS1} neurons, which are not OXT+ cells, via ARH-independent mechanisms, whereas it increases c-Fos in $PVH^{OXT/NOS1}$ neurons via ARH-dependent mechanisms, despite centrally-injected Fr-ghrelin labels a subset of both types of NO-producing neurons. The ARH-dependent ghrelin-induced activation of $PVH^{OXT/NOS1}$ neurons may involve $ARH^{AgRP/NPY}$ neurons, which are enriched in GHSR, sense plasma ghrelin and densely innervate the PVH [30–33]. $ARH^{AgRP/NPY}$ neurons target a subset of NOS1-expressing PVH neurons that expresses receptors for AgRP and NPY [61,62]. Also, $ARH^{AgRP/NPY}$ neurons innervate and inhibit a subset of PVH^{OXT} neurons, which mediate the orexigenic effects of $ARH^{AgRP/NPY}$ neuronal activation [30]. The low dose of systemically-injected ghrelin also induces c-Fos in the $ARH^{AgRP/NPY}$ neurons and feeding [36] but such effect does not seem to be sufficient to induce c-Fos in the PVH, an observation that is in line with the concept that selective activation of $ARH^{AgRP/NPY}$ neurons results in inhibition of food intake regulating PVH neurons [30]. These observations, together with previous studies [24], support the notion that high doses of systemically-injected ghrelin targets a subset of PVH neurons to activate HPA axis that is different than the subset of PVH neurons

recruited by ARH$^{AgRP/NPY}$ neurons to induce food intake. Thus, ghrelin-mediated recruitment of PVH$^{OXT/NOS1}$ and PVH^{NOS1} neurons seems to involve not only the local action of the hormone but also additional indirect mechanisms that remain to be studied.

It is well documented that ghrelin infusion increases plasma cortisol concentration in humans [63–65]. In mice, centrally- and systemically-injected ghrelin increases c-Fos in PVH^{CRH} neurons and plasma corticosterone levels [22]. Such ghrelin-induced activation of the PVH^{CRH} neurons in mice is indirect, since PVH^{CRH} neurons lack GHSR [17,22] (as confirmed here), and does not require the ARH integrity, as it is observed in ARH-ablated mice [24]. Even so, the molecular bases mediating ghrelin-induced activation of mouse PVH^{CRH} neurons remain uncertain. Previous studies in mice showed that ICV infusion of ghrelin increases NOS activity in the hypothalamus and that L-NAME reduces ghrelin-induced food intake [66,67]. Also, NOS1 knockout (KO) mice do not increase food intake in response to ghrelin [68], and NOS1 inhibition blocks ghrelin's ability to induce reward-related behaviors in rats [69]. Besides, several evidences indicate that NO activates PVH^{CRH} neurons. For instance, NO depolarizes rat type II PVH neurons that include the hypophysiotropic PVH^{CRH} neurons [70,71]. In rat PVH cultures, NO induces CRH release and NOS inhibitors reduce CRH release induced by noradrenaline, IL-1beta, IL-2 and cholinergic agonists [50,72,73]. HPA axis activation in rats induced by adrenergic receptor agonists is reduced by L-NAME or 7-nitroindazole, a specific NOS1 inhibitor [74]. The observations that systemically-injected ghrelin can reach the PVH and activate NOS1+ neurons led us to hypothesize that NO could mediate ghrelin-induced activation of the PVH^{CRH} neurons. Here, we found that L-NAME fully abrogates ghrelin-induced increase of calcium levels in PVH^{CRH} neurons and partially reduces ghrelin-induced increase of plasma corticosterone levels suggesting that indeed ghrelin-induced activation of the HPA axis involves NO signaling. Ghrelin may increase corticosterone levels, in part, via the PVH^{AVP} neurons, a fraction of which is labeled by Fr-ghrelin and control the adrenocorticotrophic hormone release from the pituitary [75]. Also, it is possible that different experimental conditions could have made more evident the role of NO signaling on the HPA axis activation at systemic level (e.g., use of selective NOS1 inhibitors, higher doses, chronic treatment, etc.). Strikingly, the lack of endogenous ghrelin signaling in genetically-modified mice was found to either impair or enhance the activation of the PVH^{CRH} neurons [17,76,77]. Thus, future studies are required to further investigate the extent to which current observations in non-stressed mice treated with ghrelin also take place when endogenous ghrelin levels fluctuate under physiological or stress conditions.

Ghrelin targets different PVH neurons and affects a variety of neurobiological mechanisms within this hypothalamic area [12,78]. Here, we propose that ghrelin action in the mouse PVH results

in production of NO that has important functional implications at a local level. The NO rapidly diffuses through the brain tissue and affects neighboring cells in a radius of ~150 µm [79,80]. Indeed, selective activation of NOS1-expressing neurons of the PVH using pharmacogenetics results in c-Fos induction not only in NOS-expressing cells but also in neighboring PVH neurons [11]. Thus, it is likely that the release of NO by ~800 NOS1+ cells within the PVH in response to systemically-injected ghrelin (as estimated based on c-Fos induction) is sufficient to impact on a significant number of neurons and terminals within the nucleus. Here, we systemically-injected L-NAME, but the short half-life of NO (~1-seg [79]) makes very unlikely that extra-PVH NO could impact on our observations. It remains to be established if the putative release of NO affects the PVH^{CRH} neurons directly or indirectly, via regulation of GABA inputs innervating them that are known to integrate multiple signals and shape PVH^{CRH} neurons activity [81,82]. PVH GABA inputs are susceptible to NO since the intra-PVH injections of a GABAA receptor antagonist prevent the sympathetic effects of intra-PVH injected NO donors [83]. Of note, we found that systemically-injected ghrelin does not affect *Nos1* mRNA levels in the PVH, but rather increases NOS1 protein phosphorylation. Also, systemically-injected ghrelin increased intracellular calcium in PVH^{CRH} neurons but not affect *Crh* mRNA levels in the PVH, unlike our previous study showing that ICV-injected ghrelin increases *Crh* mRNA levels in the PVH [22]. Conversely, systemically-injected ghrelin increases *c-Fos* mRNA levels in the PVH. Thus, it seems that systemic ghrelin treatment primarily induces rapid regulatory effects in the signaling pathways of the PVH but not gene expression, which was restricted to c-Fos, a transcription factor that likely modulates later transcriptional effects in PVH neurons.

In summary, current studies help to gain insights regarding the neurobiological basis by which ghrelin acts in the PVH and activates the HPA axis in male mice. It is important to highlight that the current study was performed on exclusively males because ghrelin is known to display stronger orexigenic effects in males than in females, in both rats and mice [84,85]. However, the HPA axis usually mediates more rapid and greater responses in females [86]. Thus, future studies should be performed to investigate if the reported observations regarding to the action of ghrelin in the PVH involve any type of sex dependent differences.

Acknowledgements

This work was supported by grants from Fondo para la Investigación Científica y Tecnológica (FONCyT, PICT2017-3196, PICT2019-3054 and PICT2020-3270 to MP), The National Qatar Research Foundation (NPRP13S-0209-200315 to MP) and Fundação de Amparo a Pesquisa do Estado de São Paulo (FAPESP, 19/27581-0 and 16/17968-6, to ASM and RR, respectively). We would like to thank to Dr. A. Abizaid (Carleton University), Dr. E Nillni (Brown University), Dr. H Gainer (National Institute of Health of US), Dr. Castro (Michigan University) for providing the antibodies against neurotensin, TRH, oxytocin/AVP, and CRH respectively. Also, we would also like to thank to Dr. M.J. Tolosa, Dr. G. García Romero, Mirta Reynaldo, Lucas Aguilar and Cintia Bruno for their technical assistance.

Disclosure Statement: The authors have nothing to disclose.

Data Availability

Some or all datasets generated during and/or analyzed during the current study are not publicly available but are available from the corresponding author on reasonable request.

REFERENCES

1. Howard AD, Feighner SD, Cully DF, et al. A receptor in pituitary and hypothalamus that functions in growth hormone release. *Science*. 1996;273(5277):974-977. doi:10.1126/science.273.5277.974

2. Kojima M, Hosoda H, Date Y, Nakazato M, Matsuo H, Kangawa K. Ghrelin is a growth-hormone-releasing acylated peptide from stomach. *Nature*. 1999;402(6762):656-660. doi:10.1038/45230

3. Giorgioni G, Del Bello F, Quaglia W, et al. Advances in the Development of Nonpeptide Small Molecules Targeting Ghrelin Receptor. *J Med Chem*. 2022;65(4):3098-3118. doi:10.1021/acs.jmedchem.1c02191

4. Graf SA, Garcia JM. Anamorelin hydrochloride in the treatment of cancer anorexia–cachexia syndrome: design, development, and potential place in therapy. *Drug Des Devel Ther*. 2017;11:2325-2331. doi:10.2147/DDDT.S110131

5. Broglio F, Arvat E, Benso A, et al. Ghrelin, a natural GH secretagogue produced by the stomach, induces hyperglycemia and reduces insulin secretion in humans. *J Clin Endocrinol Metab*. 2001;86(10):5083-5086. doi:10.1210/jcem.86.10.8098

6. Biag J, Huang Y, Gou L, et al. Cyto- and chemoarchitecture of the hypothalamic paraventricular nucleus in the C57BL/6J male mouse: a study of immunostaining and multiple fluorescent tract tracing. *J Comp Neurol*. 2012;520(1):6-33. doi:10.1002/cne.22698

7. Sawchenko PE, Swanson LW. The organization of forebrain afferents to the paraventricular and supraoptic nuclei of the rat. *J Comp Neurol*. 1983;218(2):121-144. doi:10.1002/cne.902180202

8. Miyagawa A, Okamura H, Ibata Y. Coexistence of oxytocin and NADPH-diaphorase in magnocellular neurons of the paraventricular and the supraoptic nuclei of the rat hypothalamus. *Neurosci Lett*. 1994;171(1-2):13-16. doi:10.1016/0304-3940(94)90592-4

9. Sánchez F, Alonso JR, Arévalo R, Blanco E, Aijón J, Vázquez R. Coexistence of NADPH-diaphorase with vasopressin and oxytocin in the hypothalamic magnocellular neurosecretory nuclei of the rat. *Cell Tissue Res*. 1994;276(1):31-34. doi:10.1007/BF00354781

10. Nylén A, Skagerberg G, Alm P, Larsson B, Holmqvist B, Andersson KE. Nitric oxide synthase in the hypothalamic paraventricular nucleus of the female rat; organization of spinal projections and coexistence with oxytocin or vasopressin. *Brain Res*. 2001;908(1):10-24. doi:10.1016/s0006-8993(01)02539-2

11. Sutton AK, Pei H, Burnett KH, Myers MG, Rhodes CJ, Olson DP. Control of Food Intake and Energy Expenditure by Nos1 Neurons of the Paraventricular Hypothalamus. *J Neurosci*. 2014;34(46):15306-15318. doi:10.1523/JNEUROSCI.0226-14.2014

12. Dos-Santos RC, Reis LC, Perello M, Ferguson AV, Mecawi AS. The actions of ghrelin in the paraventricular nucleus: energy balance and neuroendocrine implications. *Ann N Y Acad Sci*. 2019;1455(1):81-97. doi:10.1111/nyas.14087

13. Zigman JM, Jones JE, Lee CE, Saper CB, Elmquist JK. Expression of Ghrelin Receptor mRNA in the Rat and the Mouse Brain. *J Comp Neurol*. 2006;494(3):528-548. doi:10.1002/cne.20823

14. Perello M, Scott MM, Sakata I, et al. Functional implications of limited leptin receptor and ghrelin receptor coexpression in the brain. *Journal of Comparative Neurology*. 2012;520(2):281-294. doi:10.1002/cne.22690

15. Mani BK, Walker AK, Lopez Soto EJ, et al. Neuroanatomical characterization of a growth hormone secretagogue receptor-green fluorescent protein reporter mouse. *J Comp Neurol*. 2014;522(16):3644-3666. doi:10.1002/cne.23627

16. Cabral A, Fernandez G, Perello M. Analysis of brain nuclei accessible to ghrelin present in the cerebrospinal fluid. *Neuroscience*. 2013;253:406-415. doi:10.1016/j.neuroscience.2013.09.008

17. Spencer SJ, Xu L, Clarke MA, et al. Ghrelin regulates the hypothalamic-pituitary-adrenal axis and restricts anxiety after acute stress. *Biol Psychiatry*. 2012;72(6):457-465. doi:10.1016/j.biopsych.2012.03.010

18. Kuo YT, Parkinson JRC, Chaudhri OB, et al. The temporal sequence of gut peptide CNS interactions tracked in vivo by magnetic resonance imaging. *J Neurosci*. 2007;27(45):12341-12348. doi:10.1523/JNEUROSCI.2391-07.2007

19. Pirnik Z, Bundziková J, Holubová M, et al. Ghrelin agonists impact on Fos protein expression in brain areas related to food intake regulation in male C57BL/6 mice. *Neurochem Int*. 2011;59(6):889-895. doi:10.1016/j.neuint.2011.08.001

20. Cabral A, Valdivia S, Fernandez G, Reynaldo M, Perello M. Divergent neuronal circuitries underlying acute orexigenic effects of peripheral or central ghrelin: critical role of brain accessibility. *J Neuroendocrinol*. 2014;26(8):542-554. doi:10.1111/jne.12168

21. De Francesco PN, Fernandez G, Uriarte M, et al. Systemic Ghrelin Treatment Induces Rapid, Transient, and Asymmetric Changes in the Metabolic Activity of the Mouse Brain. *Neuroendocrinology*. 2023;113(1):64-79. doi:10.1159/000526245

22. Cabral A, Suescun O, Zigman JM, Perello M. Ghrelin indirectly activates hypophysiotropic CRF neurons in rodents. *PLoS One*. 2012;7(2):e31462. doi:10.1371/journal.pone.0031462

23. Cowley MA, Smith RG, Diano S, et al. The distribution and mechanism of action of ghrelin in the CNS demonstrates a novel hypothalamic circuit regulating energy homeostasis. *Neuron*. 2003;37(4):649-661. doi:10.1016/s0896-6273(03)00063-1

24. Cabral A, Portiansky E, Sánchez-Jaramillo E, Zigman JM, Perello M. Ghrelin activates hypophysiotropic corticotropin-releasing factor neurons independently of the arcuate nucleus. *Psychoneuroendocrinology*. 2016;67:27-39. doi:10.1016/j.psyneuen.2016.01.027

25. Kola B, Farkas I, Christ-Crain M, et al. The orexigenic effect of ghrelin is mediated through central activation of the endogenous cannabinoid system. *PLoS One*. 2008;3(3):e1797. doi:10.1371/journal.pone.0001797

26. Edwards A, Abizaid A. Clarifying the Ghrelin System's Ability to Regulate Feeding Behaviours Despite Enigmatic Spatial Separation of the GHSR and Its Endogenous Ligand. *International Journal of Molecular Sciences*. 2017;18(4):859. doi:10.3390/ijms18040859

27. Perello M, Cabral A, Cornejo MP, De Francesco PN, Fernandez G, Uriarte M. Brain accessibility delineates the central effects of circulating ghrelin. *Journal of Neuroendocrinology*. 2019;31(7):e12677. doi:10.1111/jne.12677

28. Banks WA, Tschöp M, Robinson SM, Heiman ML. Extent and Direction of Ghrelin Transport Across the Blood-Brain Barrier Is Determined by Its Unique Primary Structure. *J Pharmacol Exp Ther*. 2002;302(2):822-827. doi:10.1124/jpet.102.034827

29. Schaeffer M, Langlet F, Lafont C, et al. Rapid sensing of circulating ghrelin by hypothalamic appetite-modifying neurons. *Proc Natl Acad Sci U S A*. 2013;110(4):1512-1517. doi:10.1073/pnas.1212137110

30. Atasoy D, Betley JN, Su HH, Sternson SM. Deconstruction of a neural circuit for hunger. *Nature*. 2012;488(7410):172-177. doi:10.1038/nature11270

31. Betley JN, Cao ZFH, Ritola KD, Sternson SM. Parallel, redundant circuit organization for homeostatic control of feeding behavior. *Cell*. 2013;155(6):1337-1350. doi:10.1016/j.cell.2013.11.002

32. Cabral A, Fernandez G, Tolosa MJ, et al. Fasting induces remodeling of the orexigenic projections from the arcuate nucleus to the hypothalamic paraventricular nucleus, in a growth hormone secretagogue receptor-dependent manner. *Mol Metab*. 2020;32:69-84. doi:10.1016/j.molmet.2019.11.014

33. Wang D, He X, Zhao Z, et al. Whole-brain mapping of the direct inputs and axonal projections of POMC and AgRP neurons. *Frontiers in Neuroanatomy*. 2015;9. Accessed July 19, 2023. https://www.frontiersin.org/articles/10.3389/fnana.2015.00040

34. Abernethy WB, Bell MA, Morris M, Moody DM. Microvascular Density of the Human Paraventricular Nucleus Decreases with Aging but Not Hypertension. *Experimental Neurology*. 1993;121(2):270-274. doi:10.1006/exnr.1993.1095

35. Uriarte M, De Francesco PN, Fernandez G, et al. Evidence Supporting a Role for the Blood-Cerebrospinal Fluid Barrier Transporting Circulating Ghrelin into the Brain. *Mol Neurobiol*. 2019;56(6):4120-4134. doi:10.1007/s12035-018-1362-8

36. Cornejo MP, Denis RGP, García Romero G, et al. Ghrelin treatment induces rapid and delayed increments of food intake: a heuristic model to explain ghrelin's orexigenic effects. *Cell Mol Life Sci*. 2021;78(19-20):6689-6708. doi:10.1007/s00018-021-03937-0

37. Madisen L, Zwingman TA, Sunkin SM, et al. A robust and high-throughput Cre reporting and characterization system for the whole mouse brain. *Nat Neurosci*. 2010;13(1):133-140. doi:10.1038/nn.2467

38. Taniguchi H, He M, Wu P, et al. A Resource of Cre Driver Lines for Genetic Targeting of GABAergic Neurons in Cerebral Cortex. *Neuron*. 2011;71(6):995-1013. doi:10.1016/j.neuron.2011.07.026

39. Uriarte M, De Francesco PN, Fernández G, et al. Circulating ghrelin crosses the blood-cerebrospinal fluid barrier via growth hormone secretagogue receptor dependent and independent mechanisms. *Mol Cell Endocrinol*. 2021;538:111449. doi:10.1016/j.mce.2021.111449

40. De Francesco PN, Valdivia S, Cabral A, et al. Neuroanatomical and functional characterization of CRF neurons of the amygdala using a novel transgenic mouse model. *Neuroscience*. 2015;289:153-165. doi:10.1016/j.neuroscience.2015.01.006

41. Perello M, Stuart R, Nillni EA. Prothyrotropin-releasing hormone targets its processing products to different vesicles of the secretory pathway. *J Biol Chem*. 2008;283(29):19936-19947. doi:10.1074/jbc.M800732200

42. Lewis EM, Stein-O'Brien GL, Patino AV, et al. Parallel Social Information Processing Circuits Are Differentially Impacted in Autism. *Neuron*. 2020;108(4):659-675.e6. doi:10.1016/j.neuron.2020.10.002

43. McGirr R, McFarland MS, McTavish J, Luyt LG, Dhanvantari S. Design and characterization of a fluorescent ghrelin analog for imaging the growth hormone secretagogue receptor 1a. *Regul Pept*. 2011;172(1-3):69-76. doi:10.1016/j.regpep.2011.08.011

44. Schindelin J, Arganda-Carreras I, Frise E, et al. Fiji: an open-source platform for biological-image analysis. *Nat Methods*. 2012;9(7):676-682. doi:10.1038/nmeth.2019

45. Paxinos G, Franklin KBJ. *The Mouse Brain in Stereotaxic Coordinates*. Academic Press; 2001.

46. Abercrombie M. Estimation of nuclear population from microtome sections. *The Anatomical Record*. 1946;94(2):239-247. doi:10.1002/ar.1090940210

47. Katakam PVG, Dutta S, Sure VN, et al. Depolarization of mitochondria in neurons promotes activation of nitric oxide synthase and generation of nitric oxide. *American Journal of Physiology-Heart and Circulatory Physiology*. 2016;310(9):H1097-H1106. doi:10.1152/ajpheart.00759.2015

48. Natarajan C, Yao SY, Zhang F, Sriram S. Activation of NOD2/RIPK2 pathway induces mitochondrial injury to oligodendrocyte precursor cells in vitro and CNS demyelination in vivo. *J Neuroimmunol*. 2013;265(1-2):51-60. doi:10.1016/j.jneuroim.2013.09.009

49. McCann SM, Karanth S, Kimura M, Yu WH, Rettori V. The role of nitric oxide (NO) in control of hypothalamic-pituitary function. *Rev Bras Biol*. 1996;56 Su 1 Pt 1:105-112.

50. McCann SM, Kimura M, Karanth S, Yu WH, Rettori V. Role of nitric oxide in the neuroendocrine responses to cytokines. *Ann N Y Acad Sci*. 1998;840:174-184. doi:10.1111/j.1749-6632.1998.tb09561.x

51. Vong L, Ye C, Yang Z, Choi B, Chua S, Lowell BB. Leptin action on GABAergic neurons prevents obesity and reduces inhibitory tone to POMC neurons. *Neuron*. 2011;71(1):142-154. doi:10.1016/j.neuron.2011.05.028

52. Xu Y, Wu Z, Sun H, et al. Glutamate Mediates the Function of Melanocortin Receptor 4 on Sim1 Neurons in Body Weight Regulation. *Cell Metabolism*. 2013;18(6):860-870. doi:10.1016/j.cmet.2013.11.003

53. Xu S, Yang H, Menon V, et al. Behavioral state coding by molecularly defined paraventricular hypothalamic cell type ensembles. *Science*. 2020;370(6514):eabb2494. doi:10.1126/science.abb2494

54. Ziegler DR, Cullinan WE, Herman JP. Organization and regulation of paraventricular nucleus glutamate signaling systems: N-methyl-D-aspartate receptors. *J Comp Neurol*. 2005;484(1):43-56. doi:10.1002/cne.20445

55. Chen S, Xu H, Dong S, Xiao L. Morpho-Electric Properties and Diversity of Oxytocin Neurons in Paraventricular Nucleus of Hypothalamus in Female and Male Mice. *J Neurosci*. 2022;42(14):2885-2904. doi:10.1523/JNEUROSCI.2494-21.2022

56. Arévalo R, Sánchez F, Alonso JR, Carreterco J, Vázquezt R, Aijón J. NADPH-diaphorase activity in the hypothalamic magnocellular neurosecretory nuclei of the rat. *Brain Research Bulletin*. 1992;28(4):599-603. doi:10.1016/0361-9230(92)90109-B

57. Calka J, Block CH. Relationship of vasopressin with NADPH-diaphorase in the hypothalamo-neurohypophysial system. *Brain Res Bull*. 1993;32(3):207-210. doi:10.1016/0361-9230(93)90177-d

58. Hatakeyama S, Kawai Y, Ueyama T, Senba E. Nitric oxide synthase-containing magnocellular neurons of the rat hypothalamus synthesize oxytocin and vasopressin and express Fos following stress stimuli. *Journal of Chemical Neuroanatomy*. 1996;11(4):243-256. doi:10.1016/S0891-0618(96)00166-4

59. Steuernagel L, Lam BYH, Klemm P, et al. HypoMap-a unified single-cell gene expression atlas of the murine hypothalamus. *Nat Metab*. 2022;4(10):1402-1419. doi:10.1038/s42255-022-00657-y

60. Xiao M, Ding J, Wu L, et al. The distribution of neural nitric oxide synthase-positive cerebrospinal fluid-contacting neurons in the third ventricular wall of male rats and coexistence with vasopressin or oxytocin. *Brain Res*. 2005;1038(2):150-162. doi:10.1016/j.brainres.2005.01.032

61. Péterfi Z, Farkas I, Denis RGP, et al. Endocannabinoid and nitric oxide systems of the hypothalamic paraventricular nucleus mediate effects of NPY on energy expenditure. *Mol Metab*. 2018;18:120-133. doi:10.1016/j.molmet.2018.08.007

62. Fetissov SO, Byrne LC, Hassani H, Ernfors P, Hökfelt T. Characterization of neuropeptide Y Y2 and Y5 receptor expression in the mouse hypothalamus. *J Comp Neurol*. 2004;470(3):256-265. doi:10.1002/cne.11047

63. Takaya K, Ariyasu H, Kanamoto N, et al. Ghrelin strongly stimulates growth hormone release in humans. *J Clin Endocrinol Metab*. 2000;85(12):4908-4911. doi:10.1210/jcem.85.12.7167

64. Arvat E, Maccario M, Di Vito L, et al. Endocrine activities of ghrelin, a natural growth hormone secretagogue (GHS), in humans: comparison and interactions with hexarelin, a nonnatural peptidyl GHS, and GH-releasing hormone. *J Clin Endocrinol Metab*. 2001;86(3):1169-1174. doi:10.1210/jcem.86.3.7314

65. Tong J, Prigeon RL, Davis HW, Bidlingmaier M, Tschöp MH, D'Alessio D. Physiologic Concentrations of Exogenously Infused Ghrelin Reduces Insulin Secretion Without Affecting Insulin Sensitivity in Healthy Humans. *J Clin Endocrinol Metab*. 2013;98(6):2536-2543. doi:10.1210/jc.2012-4162

66. Abtahi S, Mirza A, Howell E, Currie PJ. Ghrelin enhances food intake and carbohydrate oxidation in a nitric oxide dependent manner. *Gen Comp Endocrinol*. 2017;250:9-14. doi:10.1016/j.ygcen.2017.05.017

67. Gaskin FS, Farr SA, Banks WA, Kumar VB, Morley JE. Ghrelin-induced feeding is dependent on nitric oxide. *Peptides*. 2003;24(6):913-918. doi:10.1016/s0196-9781(03)00160-8

68. Morley JE, Farr SA, Sell RL, Hileman SM, Banks WA. Nitric oxide is a central component in neuropeptide regulation of appetite. *Peptides*. 2011;32(4):776-780. doi:10.1016/j.peptides.2010.12.015

69. Engel JA, Pålsson E, Vallöf D, Jerlhag E. Ghrelin activates the mesolimbic dopamine system via nitric oxide associated mechanisms in the ventral tegmental area. *Nitric Oxide*. 2023;131:1-7. doi:10.1016/j.niox.2022.12.001

70. Bains JS, Ferguson AV. Nitric oxide depolarizes type II paraventricular nucleus neurons in vitro. *Neuroscience*. 1997;79(1):149-159. doi:10.1016/s0306-4522(96)00670-7

71. Ferguson AV, Latchford KJ, Samson WK. The Paraventricular Nucleus of the Hypothalamus A Potential Target for Integrative Treatment of Autonomic Dysfunction. *Expert Opin Ther Targets*. 2008;12(6):717-727. doi:10.1517/14728222.12.6.717

72. Hsieh CH, Li HY, Chen JC. Nitric oxide and interleukin-1beta mediate noradrenergic induced corticotrophin-releasing hormone release in organotypic cultures of rat paraventricular nucleus. *Neuroscience*. 2010;165(4):1191-1202. doi:10.1016/j.neuroscience.2009.12.003

73. Karanth S, Lyson K, McCann SM. Role of nitric oxide in interleukin 2-induced corticotropin-releasing factor release from incubated hypothalami. *Proc Natl Acad Sci U S A*. 1993;90(8):3383-3387. doi:10.1073/pnas.90.8.3383

74. Gadek-Michalska A, Bugajski J. Nitric oxide in the adrenergic-and CRH-induced activation of hypothalamic-pituitary-adrenal axis. *J Physiol Pharmacol*. 2008;59(2):365-378.

75. Antoni FA. Magnocellular Vasopressin and the Mechanism of "Glucocorticoid Escape." *Front Endocrinol (Lausanne)*. 2019;10:422. doi:10.3389/fendo.2019.00422

76. Fernandez G, Cabral A, De Francesco PN, et al. GHSR controls food deprivation-induced activation of CRF neurons of the hypothalamic paraventricular nucleus in a LEAP2-dependent manner. *Cell Mol Life Sci*. 2022;79(5):277. doi:10.1007/s00018-022-04302-5

77. Stark R, Santos VV, Geenen B, et al. Des-Acyl Ghrelin and Ghrelin O-Acyltransferase Regulate Hypothalamic-Pituitary-Adrenal Axis Activation and Anxiety in Response to Acute Stress. *Endocrinology*. 2016;157(10):3946-3957. doi:10.1210/en.2016-1306

78. Dos-Santos RC, Grover HM, Reis LC, Ferguson AV, Mecawi AS. Electrophysiological Effects of Ghrelin in the Hypothalamic Paraventricular Nucleus Neurons. *Frontiers in Cellular Neuroscience*. 2018;12. Accessed August 4, 2023. https://www.frontiersin.org/articles/10.3389/fncel.2018.00275

79. Garthwaite J. Concepts of neural nitric oxide-mediated transmission. *Eur J Neurosci*. 2008;27(11):2783-2802. doi:10.1111/j.1460-9568.2008.06285.x

80. Wood J, Garthwaite J. Models of the diffusional spread of nitric oxide: implications for neural nitric oxide signalling and its pharmacological properties. *Neuropharmacology*. 1994;33(11):1235-1244. doi:10.1016/0028-3908(94)90022-1

81. Boudaba C, Szabó K, Tasker JG. Physiological Mapping of Local Inhibitory Inputs to the Hypothalamic Paraventricular Nucleus. *J Neurosci*. 1996;16(22):7151-7160. doi:10.1523/JNEUROSCI.16-22-07151.1996

82. Ziegler DR, Herman JP. Local Integration of Glutamate Signaling in the Hypothalamic Paraventricular Region: Regulation of Glucocorticoid Stress Reponses. *Endocrinology*. 2000;141(12):4801-4804. doi:10.1210/endo.141.12.7949

83. Zhang K, Patel KP. Effect of nitric oxide within the paraventricular nucleus on renal sympathetic nerve discharge: role of GABA. *Am J Physiol*. 1998;275(3):R728-734. doi:10.1152/ajpregu.1998.275.3.R728

84. Clegg DJ, Brown LM, Zigman JM, et al. Estradiol-dependent decrease in the orexigenic potency of ghrelin in female rats. *Diabetes*. 2007;56(4):1051-1058. doi:10.2337/db06-0015

85. de Souza GO, Wasinski F, Donato J. Characterization of the metabolic differences between male and female C57BL/6 mice. *Life Sciences*. 2022;301:120636. doi:10.1016/j.lfs.2022.120636

86. Heck AL, Handa RJ. Sex differences in the hypothalamic–pituitary–adrenal axis' response to stress: an important role for gonadal hormones. *Neuropsychopharmacology*. 2019;44(1):45-58. doi:10.1038/s41386-018-0167-9

87. Larsson J, Godfrey AJR, Gustafsson P, algorithms) DHE (geometric, code) EH (root solver, Privé F. eulerr: Area-Proportional Euler and Venn Diagrams with Ellipses. Published online December 10, 2022. Accessed July 28, 2023. https://cran.r-project.org/web/packages/eulerr/index.html

LEGENDS

Figure 1. A. Schematic diagrams from the Mouse Brain Atlas [45] showing coronal brain sections containing different rostro-caudal levels of the PVH (between bregma -0.58 mm and -1.22 mm). **B.** Representative images of coronal brain sections containing the PVH of WT mice ICV-injected with Fr-ghrelin (pseudo-colored to cyan). Subdivisions of the PVH are overlayed following the delineation described in the Mouse Brain Atlas [45]. fx: fornix, PaAP: PVH anterior parvicellular part, PaDC: PVH dorsal cap, PaLM: PVH lateral magnocellular part, PaMM: PVH medial magnocellular part, PaMP: PVH medial parvicellular part, PaPo: PVH posterior part, PaV: PVH ventral part, pe: periventricular hypothalamic nucleus, V: third ventricle. **C-E.** Representative high magnification images of Fr-ghrelin+ cells in the PVH (**C**) and fiber-like structures in the periventricular region of the PVH of WT mice ICV-injected with Fr-ghrelin (**D-E**). Arrows point to Fr-ghrelin+ cells and arrow-heads point to Fr-ghrelin+ fiber-like structures. **F.** Representative images of brain coronal sections containing the PVH of Gad2^{tdTomato} (red) or WT mice ICV-injected with Fr-ghrelin subjected to a fluorescent immunostaining against diverse neuropeptides including CRH, TRH, AVP, NT, TH, OXT or NOS1 (red), respectively. Insets depict high magnification of areas marked in low magnification images. Arrows point dual-labelled cells (Fr-ghrelin/OXT+ or Fr-ghrelin/NOS1+) and arrow-heads point single-labelled cells (OXT+ or NOS1+). Scale bars: 100 µm (low magnification) and 20 µm (high magnification). Cell nuclei labelled with Hoechst (blue).

Figure 2. A. Representative images of coronal brain sections containing the PVH of WT mice ICV-injected with Fr-ghrelin (pseudo-colored to cyan) and subjected to a double-fluorescent immunostaining against OXT (red) and NOS1 (green). Inset depict a high magnification of the area marked in low magnification image. Arrows point to triple-labelled cells (Fr-ghrelin/OXT/NOS1+). Scale bars: 50 µm (low magnification) and 20 µm (high magnification). Cell nuclei labelled with Hoechst (blue). **B.** Venn diagram of Fr-ghrelin+, OXT+ and NOS1+ cells in the PVH of mice. **C-E.** Plots of relative gene expression of *Ghsr (C)*, *Oxt (D)* and *Nos1* (E) in neurons classified as magnocellular or parvocellular, taken from the dataset of Lewis *et al.* [42]. Cyan circles represent neurons with non-zero relative expression (at least one read) for *Ghsr.* **F.** Venn diagram of magnocellular neurons from the same dataset, classified as *Ghsr*+, *Oxt*+ and/or *Nos1*+ when presenting a relative expression greater than zero for each respective gene. Venn diagrams were generated using eulerr (https://cran.r-project.org/package=eulerr) [87] in order to have the areas of circles and their intersections proportional to the number of neurons in each subgroup.

Figure 3. A. Representative images of brain coronal sections containing the PVH of WT mice ICV-injected with vehicle or ghrelin, respectively, subjected to a triple-immunostaining against

c-Fos (white), OXT (red) or NOS1 (green). Insets depict a high magnification image of the areas marked in low magnification images. Arrows point to triple-labelled cells (c-Fos/OXT/NOS1+ cells) and arrow-heads point c-Fos+ cells. Scale bars: 50 µm (low magnification) and 20 µm (high magnification). Cell nuclei labelled with Hoechst (blue). **B.** Representative greyscale images of coronal brain sections containing the PVH of WT mice ICV-injected with vehicle or ghrelin, respectively, perfused 15 min later and subjected to a chromogenic immunostaining against phospho-NOS1. Insets depict a high magnification image of the areas marked in low magnification images. Arrows point to phospho-NOS1+ cells. Scale bars: 50 µm (low magnification) and 20 µm (high magnification). **C.** Bar graph displaying the quantitative analysis of the number of phospho-NOS1+ cells in the PVH of WT mice ICV-injected with vehicle or ghrelin, respectively, and perfused 15, 30 or 120 min later. Data represent the mean±SEM and were compared by One-way ANOVA [$F_{treat}(3,9) = 59.06$, $p<0.0001$] followed by Tukey's multiple comparisons tests. ***, $p<0.001$ vs vehicle-treated group.

Figure 4. A. Representative images of coronal brain sections containing the PVH of WT mice SC-injected with vehicle, 60 pmol/g BW or 600 pmol/g BW of ghrelin, respectively, and subjected to a chromogenic immunostaining against c-Fos (black/purple). Scale bars: 100 µm. **B.** Pseudo-colored images of coronal brain sections containing the PVH of WT mice SC-injected with vehicle or F-ghrelin 600 pmol/g BW, respectively, and subjected to a chromogenic immunostaining against fluorescein. Scale bars: 100 µm. **C.** Line graph displaying the quantitative analysis of the optical density signal in a 300 µm box length placed over the PVH as shown in panel B. Data represent the mean±SEM and were compared by unpaired Student's t-test with Welch correction. *, $p<0.05$ vs vehicle-treated group.

Figure 5. A. Representative images of coronal brain sections containing the PVH of ARH-intact or ARH-ablated mice SC-injected with vehicle or 600 pmol/g BW of ghrelin, respectively, subjected to a triple-immunostaining against c-Fos (white), OXT (red) or NOS1 (green). Insets depict a high magnification image of the areas marked in low magnification images. Arrows point to triple-labelled cells (c-Fos/OXT/NOS1+ cells) and arrow-heads point to c-Fos+ cells. Scale bars: 50 µm (low magnification) and 20 µm (high magnification). Cell nuclei labelled with Hoechst (blue). **B-G.** Bar graphs displaying the quantitative analysis of the percentage of $PVH^{OXT/NOS1}$, PVH^{NOS1} and PVH^{OXT} neurons positive for c-Fos in the periventricular (**B**, **D** and **F**) or lateral region (**C**, **E** and **G**) of the PVH, respectively, of ARH-intact or ARH-ablated mice SC-treated with 600 pmol/g BW of ghrelin. Data represent as mean±SEM. Data of each neuronal set and in each PVH region were compared using both one-sample t-test vs. 0 %. to test if groups responded to ghrelin

(comparisons labeled in red **, p<0.01 and *, p<0.05), and unpaired Student's t-test to test if the magnitude of responses were different (comparison labeled in blue #, p<0.05).

Figure 6. A. Schematic view of the fiber photometry system used for recording GCaMP8m-expressing CRH neurons signal in the mouse PVH. **B.** Line graph displaying the quantitative analysis of the relative changes in fluorescence in the PVH of Crh-cre mice intra-PVH injected with a AAV.DIO-GCaMP8m virus and IP-treated with vehicle, ghrelin 60 pmol/g BW, ghrelin 600 pmol/g BW or ghrelin 600 pmol/g BW + L-NAME. The arrow indicates the time at which IP injections were performed and the dotted line indicates the time period in which fluorescence was analyzed and compared (shown in C). **C**. Bar graph showing the quantitative analysis of the relative changes in fluorescence from 10 to 20 min after IP-treatment in B. Data represent the mean±SEM and were compared by One-way ANOVA [$F_{treat}(3,16) = 2.494$, $p=0.0971$] followed by Fisher's LSD test (*, $p<0.05$). **D-E.** Bar graphs displaying the quantitative analysis of the total number of c-Fos+ cells in the PVH (**D**) and plasma corticosterone levels (**E**) of WT mice SC-treated with vehicle, L-NAME (10 µg/g BW), ghrelin (600 pmol/g BW), or ghrelin (600 pmol/g BW) + L-NAME (10 µg/g BW). Data represent the mean±SEM and were compared by One-way ANOVA (in **D** [$F_{treat}(3,14) = 13.42$, $p=0.0002$]); in **E** [$F_{treat}(3,25) = 64.53$, $p<0.0001$] followed by Tukey's multiple comparisons tests. ***, $p<0.001$ and **, $p<0.01$, vs vehicle- and L-NAME-treated group; $^{\#}$, $p<0.05$, vs ghrelin-treated group.

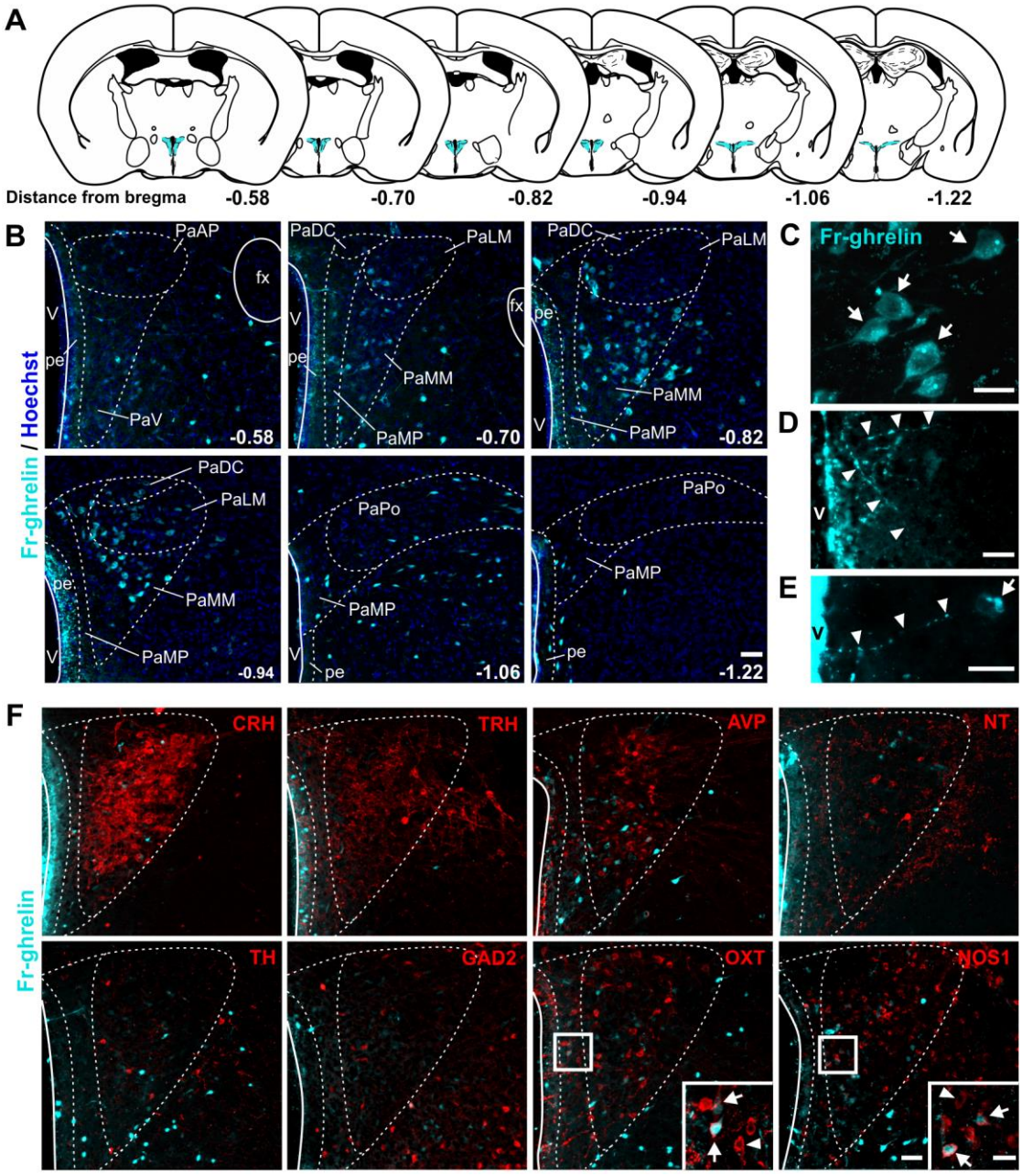
A
Distance from bregma
-0.58
-0.70
-0.82
-0.94
-1.06
-1.22
B
Fr-ghrelin / Hoechst
PaAP
fx
V
pe
PaV
PaDC
PaLM
PaMM
PaMP
PaPo
C
Fr-ghrelin
D
E
F
CRH
TRH
AVP
NT
TH
GAD2
OXT
NOS1

Figure 1

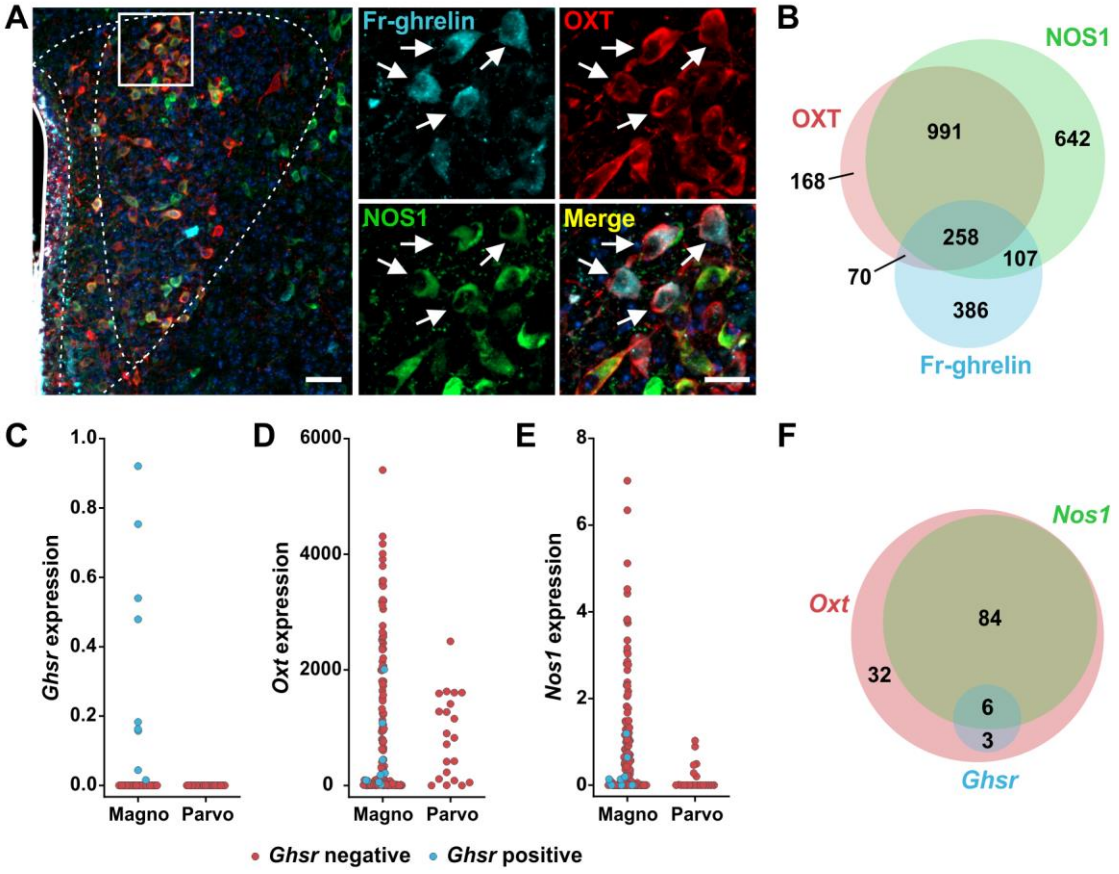
A
Fr-ghrelin
OXT
NOS1
Merge
B
NOS1
OXT
Fr-ghrelin
991
642
168
258
107
70
386
C
Ghsr expression
1.0
0.8
0.6
0.4
0.2
0.0
Magno
Parvo
D
Oxt expression
6000
4000
2000
0
Magno
Parvo
E
Nos1 expression
8
6
4
2
0
Magno
Parvo
Ghsr negative
Ghsr positive
F
Nos1
Oxt
Ghsr
84
32
6
3

Figure 2

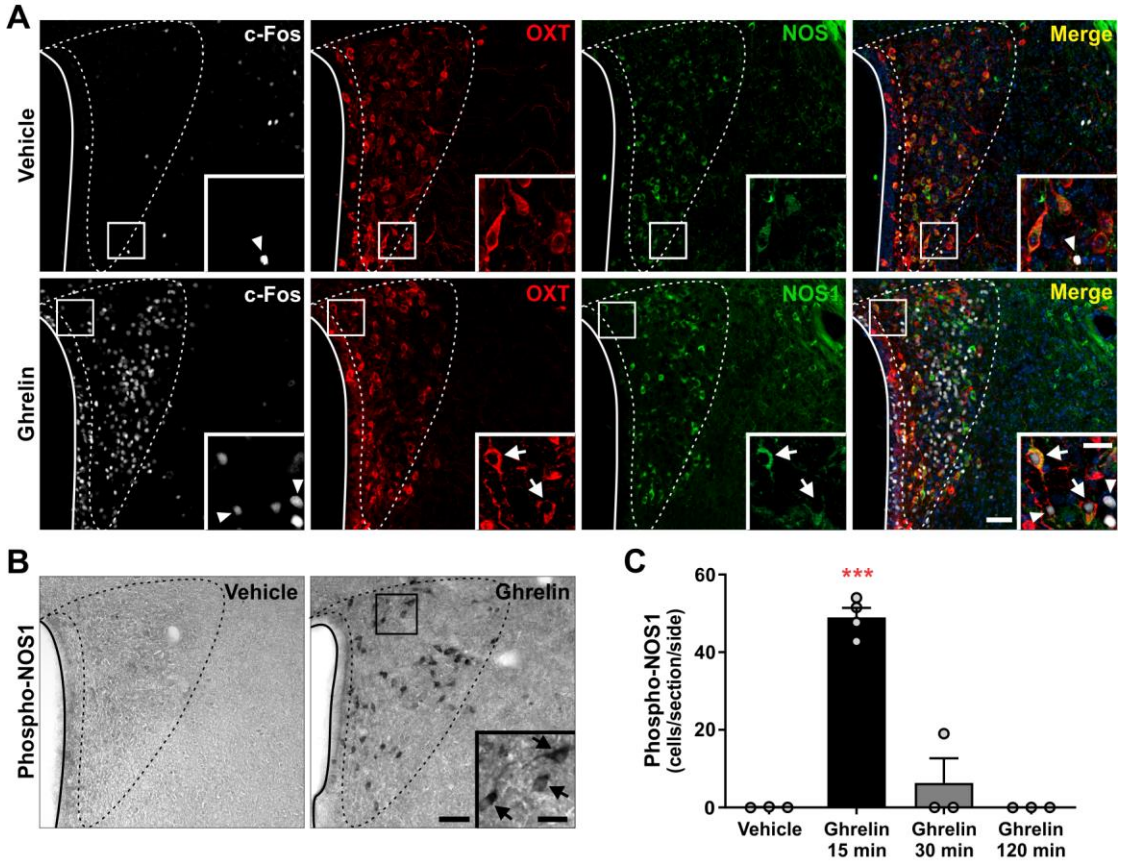
A
c-Fos
OXT
NOS1
Merge
Vehicle
Ghrelin
B
Vehicle
Ghrelin
Phospho-NOS1
C
Phospho-NOS1
(cells/section/side)
60
40
20
0
***
Vehicle
Ghrelin
15 min
Ghrelin
30 min
Ghrelin
120 min

Figure 3

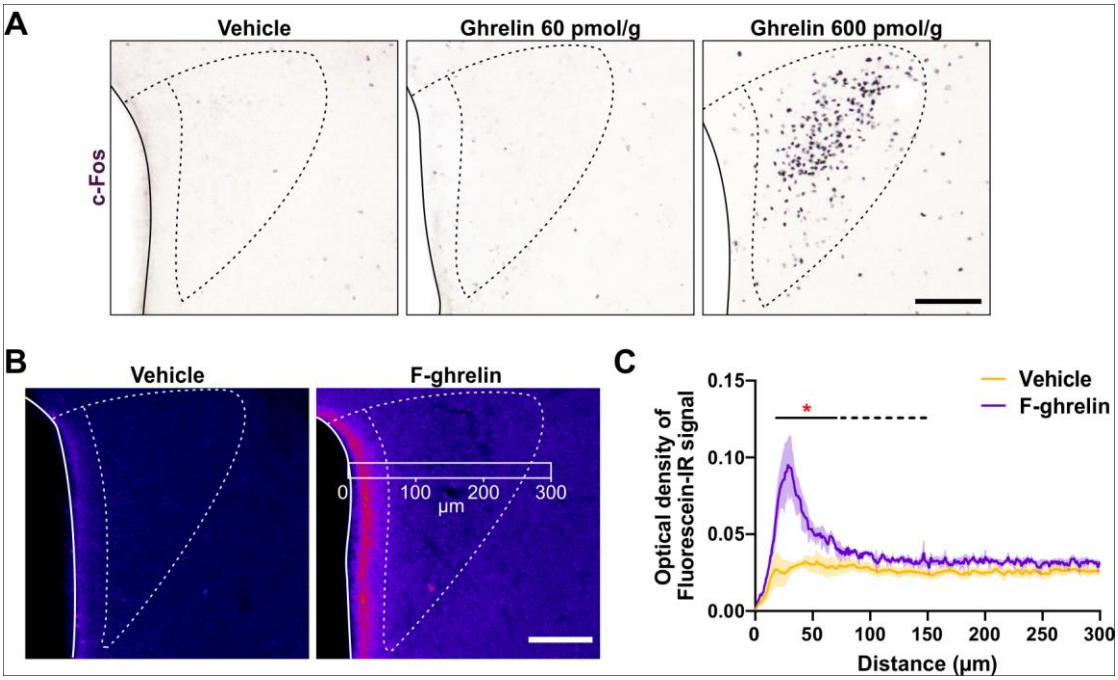
A
Vehicle
Ghrelin 60 pmol/g
Ghrelin 600 pmol/g
c-Fos
B
Vehicle
F-ghrelin
0
100
200
300
µm
C
Vehicle
F-ghrelin
Optical density of Fluorescein-IR signal
0.15
0.10
0.05
0.00
*
0
50
100
150
200
250
300
Distance (µm)

Figure 4

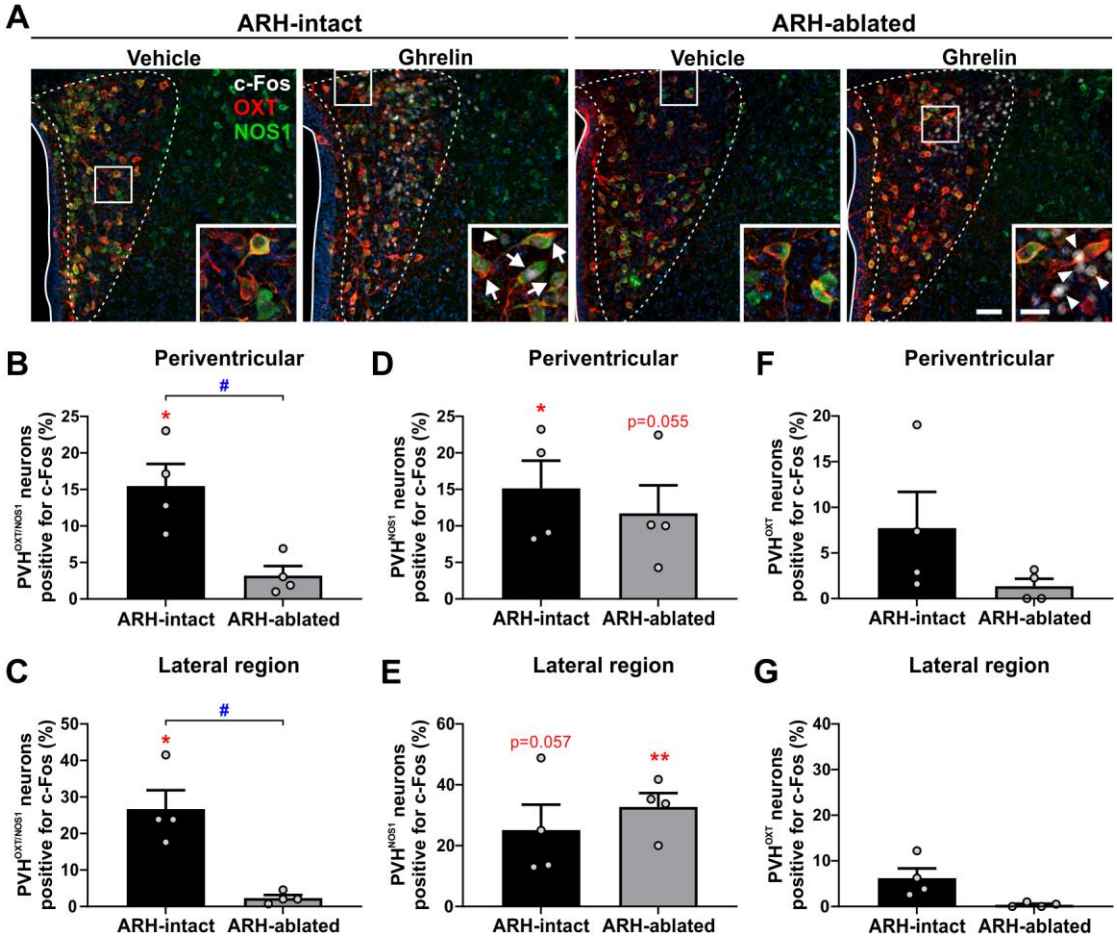
A
ARH-intact
ARH-ablated
Vehicle
Ghrelin
Vehicle
Ghrelin
c-Fos
OXT
NOS1
B
Periventricular
PVH^OXT/NOS1 neurons positive for c-Fos (%)
ARH-intact
ARH-ablated
C
Lateral region
PVH^OXT/NOS1 neurons positive for c-Fos (%)
ARH-intact
ARH-ablated
D
Periventricular
PVH^NOS1 neurons positive for c-Fos (%)
p=0.055
ARH-intact
ARH-ablated
E
Lateral region
PVH^NOS1 neurons positive for c-Fos (%)
p=0.057
ARH-intact
ARH-ablated
F
Periventricular
PVH^OXT neurons positive for c-Fos (%)
ARH-intact
ARH-ablated
G
Lateral region
PVH^OXT neurons positive for c-Fos (%)
ARH-intact
ARH-ablated

Figure 5

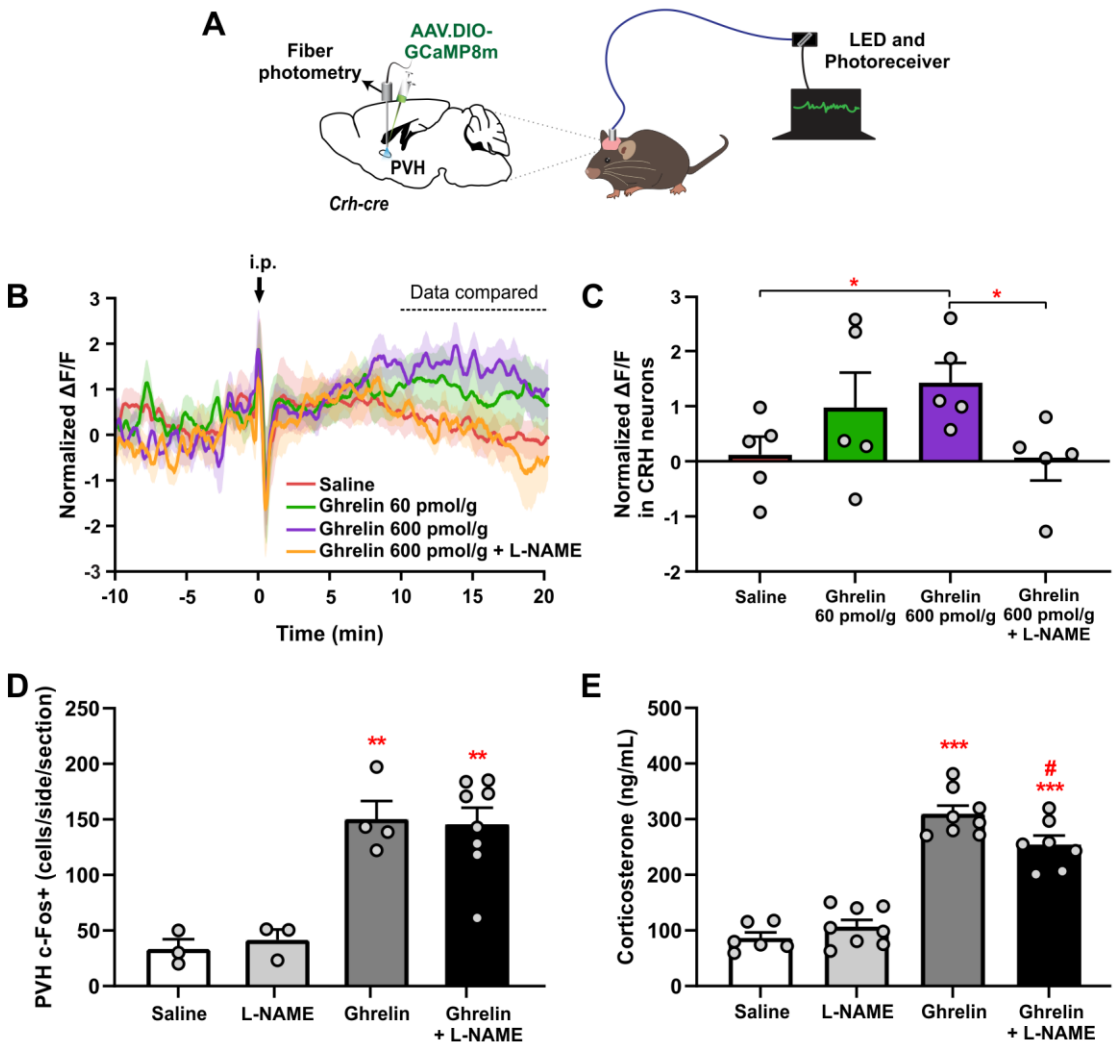
A
AAV.DIO-
GCaMP8m
Fiber
photometry
PVH
Crh-cre
LED and
Photoreceiver
B
i.p.
Data compared
Normalized ΔF/F
Saline
Ghrelin 60 pmol/g
Ghrelin 600 pmol/g
Ghrelin 600 pmol/g + L-NAME
Time (min)
C
Normalized ΔF/F
in CRH neurons
Saline
Ghrelin
60 pmol/g
Ghrelin
600 pmol/g
Ghrelin
600 pmol/g
+ L-NAME
D
PVH c-Fos+ (cells/side/section)
Saline
L-NAME
Ghrelin
Ghrelin
+ L-NAME
E
Corticosterone (ng/mL)
Saline
L-NAME
Ghrelin
Ghrelin
+ L-NAME

Figure 6